Accurate Estimation of Core Losses for PFC Inductors

by

Tobin Meyers

A Thesis Presented in Partial Fulfillment
of the Requirements for the Degree
Master of Science

Approved November 2019 by the
Graduate Supervisory Committee:

Raja Ayyanar, Chair
Jiangchao Qin
Qin Lei

ARIZONA STATE UNIVERSITY

December 2019

ABSTRACT

As the world becomes more electronic, power electronics designers have continuously designed more efficient converters. However, with the rising number of nonlinear loads (i.e. electronics) attached to the grid, power quality concerns, and emerging legislation, converters that intake alternating current (AC) and output direct current (DC) known as rectifiers are increasingly implementing power factor correction (PFC) by controlling the input current. For a properly designed PFC-stage inductor, the major design goals include exceeding minimum inductance, remaining below the saturation flux density, high power density, and high efficiency. In meeting these goals, loss calculation is critical in evaluating designs. This input current from PFC circuitry leads to a DC bias through the filter inductor that makes accurate core loss estimation exceedingly difficult as most modern loss estimation techniques neglect the effects of a DC bias. This thesis explores prior loss estimation and design methods, investigates finite element analysis (FEA) design tools, and builds a magnetics test bed setup to empirically determine a magnetic core's loss under any electrical excitation. In the end, the magnetics test bed hardware results are compared and future work needed to improve the test bed is outlined.

ACKNOWLEDGMENTS

It takes a village to raise a child. Likewise, this master's thesis belongs to the many people who helped me along the journey. Firstly, the many lessons learned over the course of this degree would not have been possible without the belief in my success and many hours invested from my advisor, Dr. Raja Ayyanar. Additionally, I would like to thank Dr. Qin Lei and Dr. Jiangchao Qin for serving as members of my master's committee and my academic advisor Toni Mengert for helping to orchestrate my success. In the classroom, Dr. Brent Sebold was instrumental in teaching me how to find problems that need solving and Barbara Haney outstanding in improving my professional skills and image.

Rarely when working at the cutting edge does an outsider offer his or her entire support so I am extremely grateful to the help provided by Jun Wang from University of Bristol. Additionally, I am grateful for the many hours of discussion and troubleshooting with my Power Electronics lab colleagues: Deliang Wu, Madhura Sondharangalla, Nikhil Korada, Ankul Gupta, Scott Mongrain, Hafsa and Haleema Qamar, and Bassam Raza. Without their challenges and encouragement, this program would have not been as beneficial to my academic development.

Even with strong professional and academic support networks, it is fantastic to have family and friends to endure the pain of knowing a graduate student. Most notably, my parents Eva and Mike Meyers, my brother Jack Meyers, my grandparents Marlene and Larry Meyers, and my girlfriend Ashley Macejko.

Finally, I am grateful to the PowerAmerica institute for funding one of my major projects, the IEEE Power and Energy Society for financially supporting both my bachelor's and master's degrees, and Arizona State University for providing the means to continuously innovate both inside and outside of the classroom.

TABLE OF CONTENTS

Page

LIST OF TABLES

Table Page

LIST OF FIGURES

Figure Page

Figure Page

Figure Page

1 INTRODUCTION & LITERATURE REVIEW

1.1 Background

Many electrical devices today rely on direct current (DC) power, however the grid operates with alternating current (AC) power. To overcome this, a converter known as a rectifier is used to convert DC to AC. Common applications of rectifiers include Uninterrupted Power Supplies (UPS), Light Emitting Diodes (LEDs), computer power supplies, phone chargers, electric vehicle chargers, data centers, home energy storage, and other digital devices [1]. Rectifiers are considered to be nonlinear loads since the voltage and current waveforms over the devices are not linearly related as they would be in a standard load such as standard light bulbs, induction motors, or electric heaters [2-4].

This nonlinearity from power electronics becomes problematic for several reasons; the most major of which are harmonics and low power factor. Harmonics are higher frequency components created by the switch-mode power supply (SMPS) rectifier that interfere with the AC grid. AC sources containing a higher percentage of harmonics can interfere and damage existing electrical loads [2-4]. These issues such as light flicker, frequent circuit breaker tripping, unnecessary fuse blowing, and damage to connected electronic components like computers are known as power quality concerns [2-4]. To protect consumers from power quality issues, two major standards exist (IEEE 519 [5] and IEC 61000-3-2 [6]) that require rectifiers over a certain power level to meet stringent harmonic levels.

The other major issue is power factor, the main application of this paper. Power factor is the ratio of real power (P) to total apparent power (S). Utilities desire the highest power factor of unity (1) where P = S but this is not always possible such as in

passive rectification circuits. However, using various SMPS topologies and control schemes, both harmonic content and power factor can be managed to meet desired goals yet all of these methods require magnetic components, specifically a filter [7].

At the simplest level, a PFC rectifier can be broken down into phases (see Figure 1.1) [8]. Firstly, the AC input has protective circuitry (i.e. fuses, varistors) before the signal is fed through an electromagnetic interference (EMI) filter to remove high frequency noise. Next, the input enters a full-wave rectifier, for example a diode bridge or switching totem-pole setup, which rectifies the sine wave. The rectified sine wave is then fed into a PFC converter stage such as a Boost PFC converter (with a PFC filter inductor) that would output a higher voltage DC signal while maintaining unity power factor. Finally, a DC link capacitor is used to smooth the voltage further before feeding into a point of load (POL) step-down converter with optional isolation that provides a lower DC voltage depending on the load and its requirements.

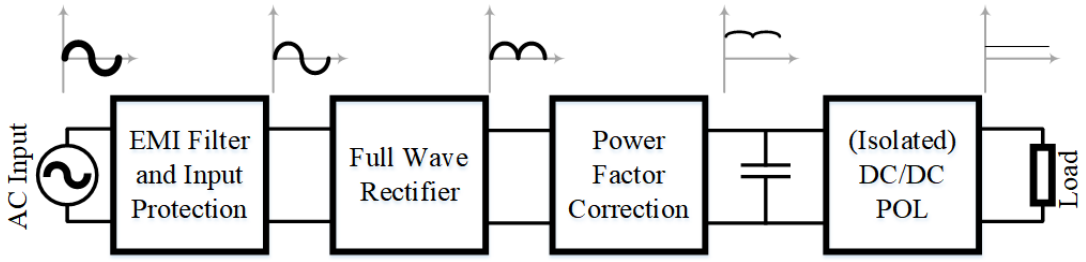

Figure 1.1: PFC Flow Chart

1.2 Magnetics Fundamentals

Transformers and inductors share many common traits, however, the main objective of an inductor is energy storage while a transformer is focused upon power transfer. Basic properties of inductors (and transformers) are explained

thoroughly in [9] but a few key concepts will be discussed here before moving on to the Power Factor Correction (PFC) inductor design.

An inductor is simply wire wrapped around a material. Inductance, the measurement of how well a core can store energy is proportional to the core's permeability (μ). A common plot to characterize a material's permeability is the B-H magnetization curve which plots the material's magnetic flux density (B) vs the material's magnetic field intensity (H). The slope of B to H is known as permeability. If the magnetization curve of air were plotted (as in Figure 1.2), the magnetization of air would be linear with a constant permeability known as the vacuum permeability or the permeability of free space (μ_o). On the other hand, if a ferromagnetic material were tested, the magnetization curve would look as shown in Figure 1.1 with free space in purple and a generic magnetic core in black. This special magnetization curve is known as a hysteresis curve which results from the alignment of magnetic dipoles due to external excitation. Because of hysteresis energy storage, it is possible to store more energy in a ferromagnetic core such as a ferrite material than simply in air. Additionally, a ferromagnetic core will provide a higher inductance for a lower number of turns due to the same phenomenon. One key metric given by the hysteresis curve is the saturation magnetic flux density (B_{sat}). At this point, the permeability becomes linear and the core is no longer useful. For this reason, cores used in high-current applications often incorporate an air gap to increase the saturation density's corresponding magnetic field intensity (H) as can be seen in Figure 1.3 where the black hysteresis loop has no air gap and the purple loop has an arbitrary air gap. Most manufacturers provide key information about the hysteresis loop which varies for various materials at different temperatures amongst other factors as demonstrated in [10].

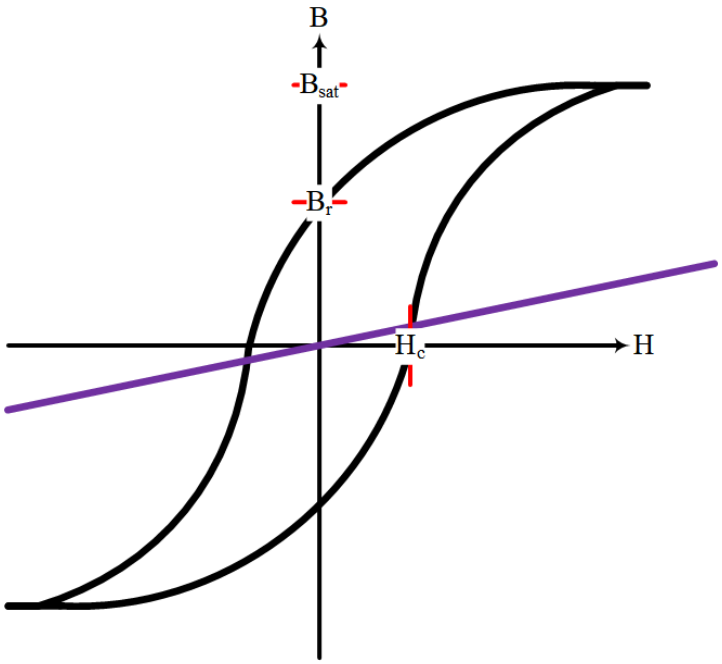

Figure 1.2: Hysteresis Curve Magnetization (Black) Compared to Free Space Magnetization (Purple)

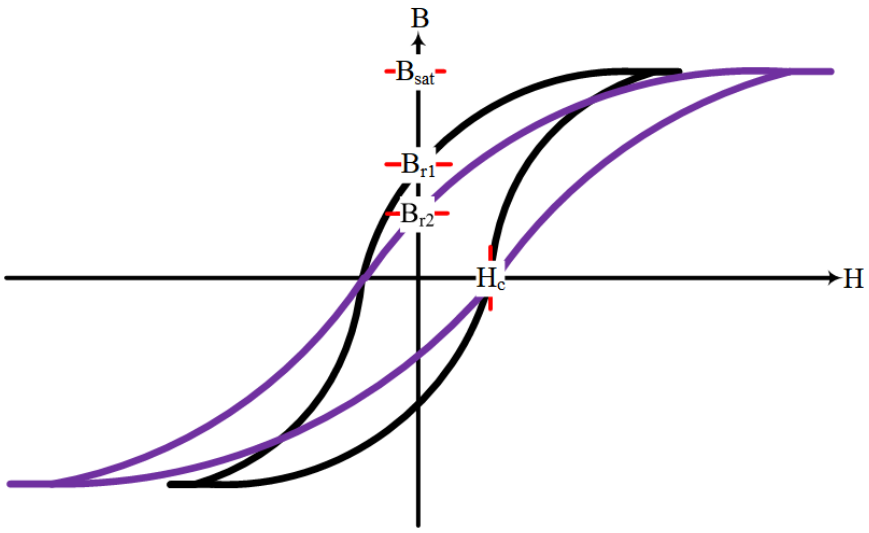

Figure 1.3: Hysteresis Curve with and without Air Gap

When designing an inductor, there are several design goals including limiting the magnetic flux density (B) below the saturation flux desnsity (B_{sat}) to prevent core saturation. In most circuits, a minimum inductance is required from the inductor which

is another minimum design goal. With those two fundamental inductor design parameters, there are several optimization factors that can determine how well an inductor was designed: most importantly, power density and efficiency. For these parameters to be fully explored and later optimized, accurate loss estimation is critical.

The simplest design technique (described very well in [9]) is to start with the accompanying circuit for parameter extraction. First, determine the lowest possible (magnetizing) inductance for overall circuit operation along with the accompanying inductor current and voltage waveforms. For leakage transformer or coupled inductor design, a specification might exist for required leakage inductance but this will require additional analysis and methods to design (i.e. FEA and short circuit test). With these parameters, [9] provides nearly algorithmic methods to choose a core material, core size, air gap, and number of turns.

Now that several options have been configured, the optimization process begins. Typical magnetic component optimization criteria are size, efficiency, and cost. For magnetic components, the loss has universally been accepted to fall into two major categories: core loss and wire loss (see Figure 1.4). Wire loss can be further classified into AC resistance and DC resistance where DC resistance is standard ohmic resistance from the conductor that can be measured. AC resistance is a modeled quantity to represent the proximity effect and skin effect predominantly. Skin effect results from current only flowing within a certain distance of the outer wire diameter proportional to frequency, known as a skin depth. Proximity effect is an additional AC agitation resulting from current-carrying wires having their magnetic fields interfere further reducing the possible current-carrying area. Skin effect can be easily mitigated by using multiple conductors with diameters roughly equal to twice the skin depth [11] but Dowell's

equation for wire loss calculation [12] accurately calculates the total AC resistance resulting from these two factors nonetheless with a high degree of accuracy unless the frequency is extremely high [11].

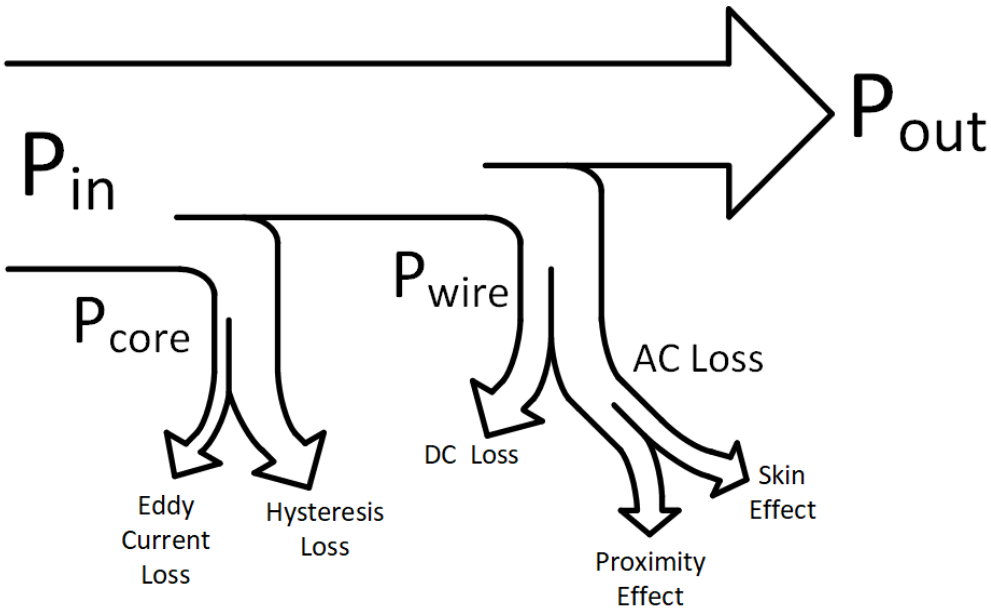

Figure 1.4: Magnetic Component Loss Breakdown

On the other hand, core loss is significantly more complicated. The older breakdown of core loss was simply eddy current loss in the core material and hysteresis loss, however, with modern ferrites' high resistivity, the eddy current loss is virtually zero. Most core manufacturers provide loss curves in their data sheets as a function of maximum magnetic flux density (B_{max}) for various discrete frequencies obtained through sinusoidal excitation of the core material as demonstrated in [10]. Through usage of the Steinmetz Equation, any circuit can have its loss calculated through interpolation of the datasheet's parameters for arbitrary waveforms. The Steinmetz equation has evolved to account for more factors with the most recent version being the Improved Improved Generalized Steinmetz Equation (i^2GSE) [13]. This equation adapts the loss curves

calculated using sinusoidal excitation for usage with the pulse excitations commonly used in switch-mode power electronics (SMPS). Despite the many existing tools that can compare cores (as discussed in the PLECS- and Ansys-based Analysis section), difficulties still arise when DC bias or leakage inductance are needed as design parameters.

1.3 Power Factor Correction Core Design

Over a fully rectified sine wave cycle, the inductor's inductance (L), magnetic flux density (B), and loss (P) all vary due to the inherent DC bias. This makes the inductor design more difficult than a standard DC-DC converter. Regardless, the same methods can be applied to the PFC inductor design while accounting for the worst case qualities. For example, the highest magnetic flux density (B_{max}) will be occurring over every period for a DC-DC inductor while the PFC inductor's B_{max} occurs at the highest B of the period for the sine wave's maximum period which will be used in determining the number of turns and air gap to prevent core saturation. A similar analysis can be done for determining the L_{min} by specifying the minimum inductance as a design parameter. The inductance also can be easily validated using an RLC meter (Figure 1.5) or complex impedance analyzer (Figure 1.6). Wire loss is calculated similarly using a Fast Fourier Transform (FFT) to break the current into frequency components that are individually fed into basic wire loss equations. Yet the primary difficulty arises in calculating core loss due to the nature of magnetic hysteresis.

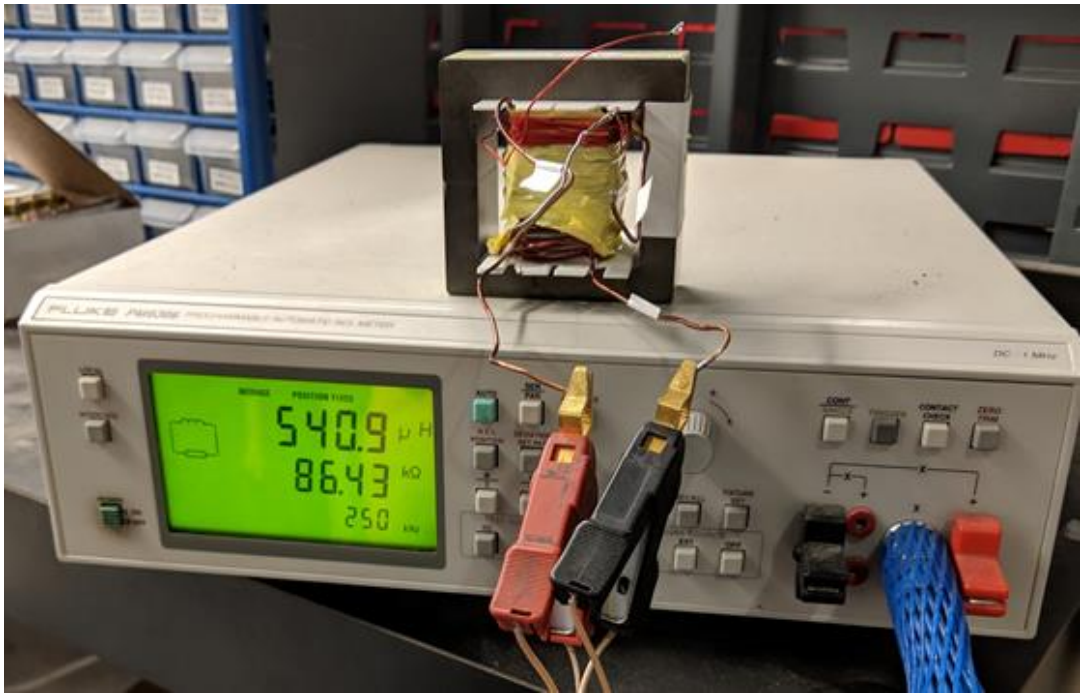

Figure 1.5: Validating Impedance with RLC Meter

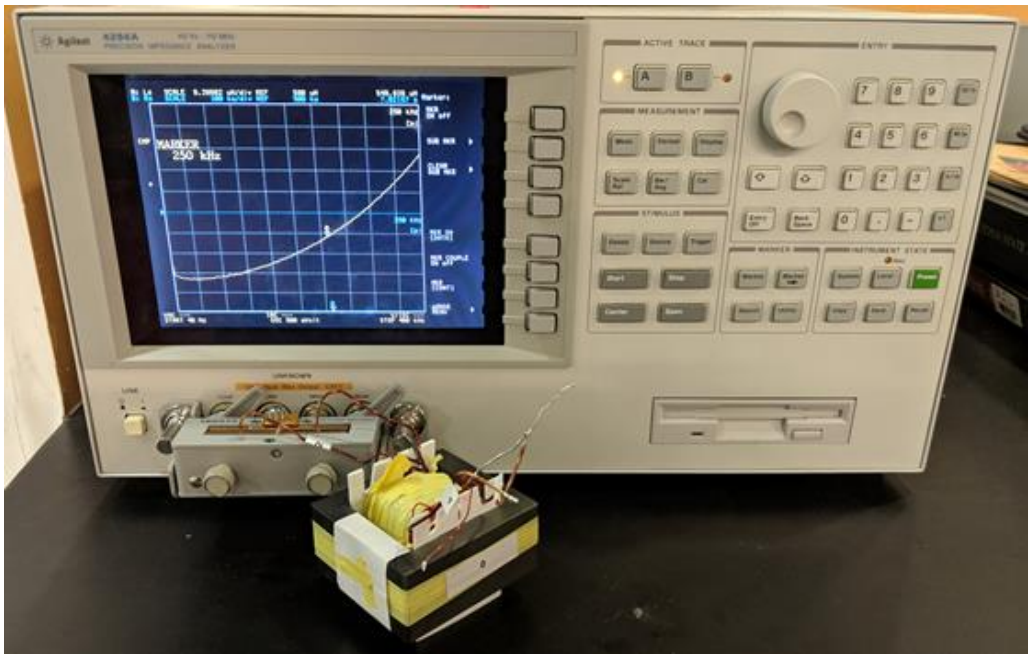

Figure 1.6: Validating Impedance with Complex Impedance Analyzer

1.4 Power Factor Correction Core Loss Estimation

As discussed previously, magnetic hysteresis is the nonlinear permeability curve that sets a ferrite core apart from an air core. When zero DC bias is applied to the core, the energy loss (in Joules) is the area enclosed by the entire hysteresis loop but when a DC bias is applied, a minor hysteresis loop moves up the major hysteresis loop and this minor loop determines the loss. Because of this different loop, standard DC-DC loss estimation techniques cannot be directly applied to PFC inductors. The most recent Steinmetz loss calculation method (i^2GSE) was integrated with Steinmetz Premagnetization Graphs (SPGs) in a way to scale basic Steinmetz parameters to account for this phenomenon [14]. This method was shown to be accurate in estimating core loss under DC bias but did not show gapped core estimation since, under this method, gapped cores require a complex reluctance model that further degrades the accuracy. Additionally, this method requires a hardware core characterization and still relies on the Steinmetz parameters (through i^2GSE) which were obtained with sinusoidal (not pulsed) excitations over a generic material (not a specific core).

A modern paper that addresses all of these concerns is [15]. In this paper, a B-H loop measurement approach is taken to simply create a loss map characterization utilizing two plots (one 1D, one 2D) that can be easily implemented with a simulator for the practicing engineer. Much like the various Steinmetz loss calculation methods (including the Steinmetz Premagnetization Graphs), [15]'s method only calculates core loss and can be used with a wire loss calculator to determine the total magnetic component's loss.

[15]'s modified B-H loop measurement method utilizes a half bridge (Figure 1.7) to excite a magnetic core with three pulses. The half bridge utilizes two separate DC

supplies that allow fine tuning to ensure voltage pulses over the magnetic core are equal in magnitude which allows the core to reach a steady-state condition. Likewise, the three pulses (Figure 1.8) are intended to set a DC core bias, settle into DC steady-state, and one full cycle to record the data. After the tests have been run, loss maps are generated using circuit domain terms such as period length, average current, and voltage pulse magnitude rather than magnetic domain terms like magnetic field intensity (H) and magnetic flux density (B) which require additional calculations. To use the loss maps in simulation, waveforms are read into a script that calculates the half-cycle quantities of period, maximum voltage magnitude, and average current which are then fed into a lookup table. At the end of the data file, all energy levels are averaged and the inductor's core loss can be found. A major component of this thesis is implementing and modifying [15]'s method to accurately determine PFC inductor loss as well as improve on several areas for improvement.

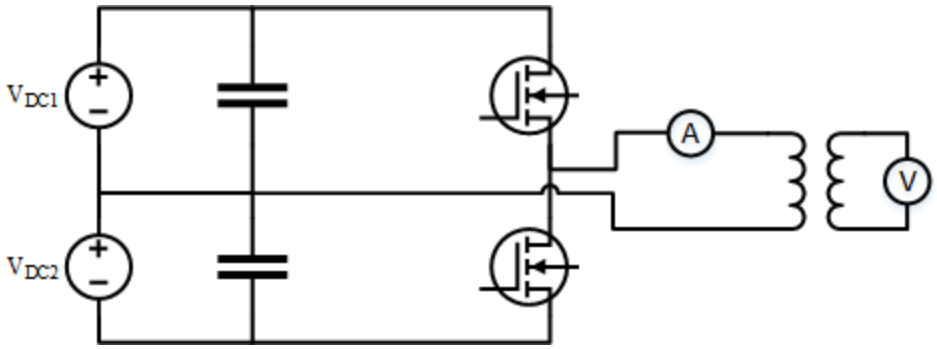

Figure 1.7: Magnetics Test Bed Half Bridge Schematic

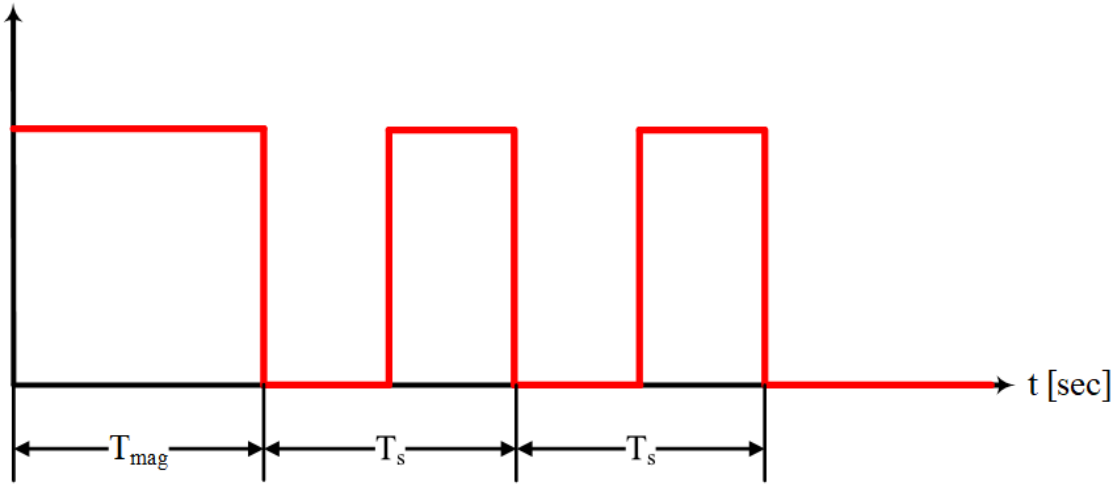

Figure 1.8: Triple Pulse Test Gate Signal

Figures 1.9 and 1.10 demonstrate ideal loss maps created by the magnetics test bed that could be used with any circuit simulator's inductor current and voltage waveforms to accurately determine the core loss with a DC bias and air gap.

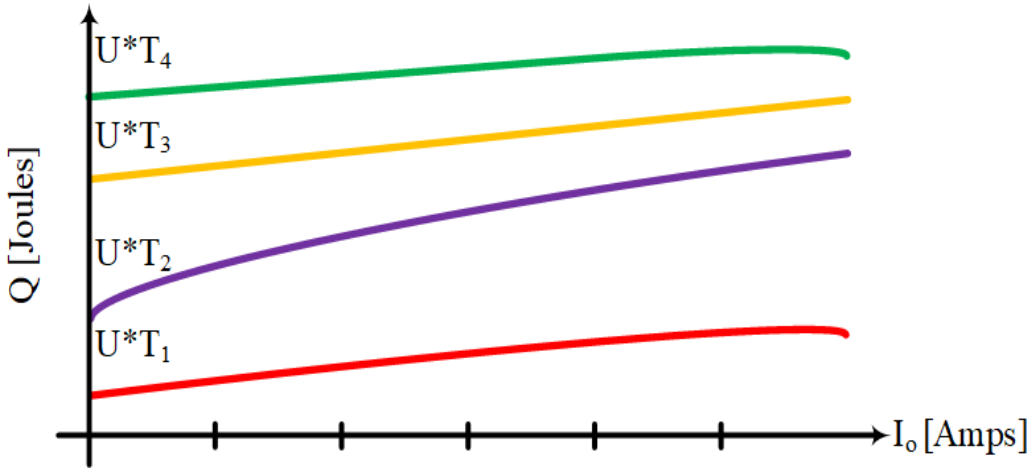

Figure 1.9: Ideal Magnetics Test Bed Loss Map

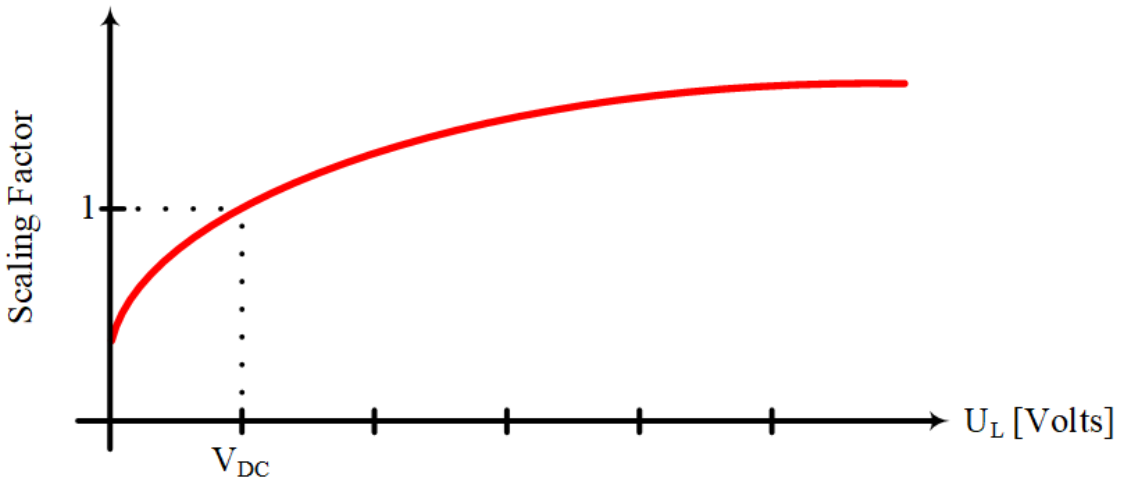

Figure 1.10: Ideal Magnetics Test Bed Scaling Map

1.5 Winding Techniques

As discussed previously, winding loss is thoroughly covered in additional material [10]. However, the actual winding method of a magnetic core can widely vary. The basic act of winding a magnetic component simply involves wrapping a conductive material around the desired magnetic leg of a core for a number of times. In determining the conductive material, the major factors are maximum voltage in determining insulation strength, maximum current in determining conductor material/thickness, and frequency to determine strand thickness.

1.5.1 Conductor Comparison

The options of conductive material include solid wire, litz wire, foil, and Printed Computer Board (PCB) traces. Solid or stranded wire which provides one solid area (even if stranded wire used since the strands are not insulated) is generally not a good choice. Especially at higher frequencies, the skin effect will give a high wire loss regardless of size, dominating the possibly low DC wire loss.

Another option is litz wire which consists of many individually insulated strands that can overcome the skin effect but becomes more expensive as the strand count increases. Litz can be tricky to connect as each strand must be soldered properly to remove the insulation and prevent underutilizing the area by leaving strands insulated. Similarly to litz, foil windings are thin copper strips insulated in a thin dielectric tape so that skin effect loss will be minimized. Foil used for winding purposes can be purchased, however, limited selection and very thin strips makes foil more difficult to use at higher power levels. PCB windings have many design techniques ranging from an affordable and flexible stacking method [16] as well as creating a multi-layered custom PCB that can be very expensive but high performance [17]. PCB manufacturing has its limits much like foil winding manufacturers so, for the scope of this thesis, it was determined that foil windings area a more economical solution to maximize copper area in the restricted winding window given that the foil can be manufactured.

1.5.2 Custom Bobbins

One advantage of PCB windings is the natural ease of assembly once they have been manufactured as they hold a fixed shape. Winding magnetic components using other conductor types (i.e. solid, litz, foil) can be difficult to maneuver without damaging the fragile ferrite core. A common practical method to quickly and easily wrap a core with the specified number of turns is a bobbin. Fundamentally, a bobbin is a dielectric shell that slides onto a magnetic core with the windings already attached. For testing, a bobbin is priceless in versatility of testing different winding combinations to see how various inductance levels can affect component efficiency. Through additive manufacturing, custom bobbins were created (Figure 1.11) with custom heights to enable a uniform core air gap and test that as an additional factor. In addition, custom winding patterns are possible such as separate primary and secondary windings that maximize

leakage inductance (Figure 1.12). Since parametric design was used in Autodesk Fusion 360 [18], the air gap can be simply changed by varying the height variable and reprinting.

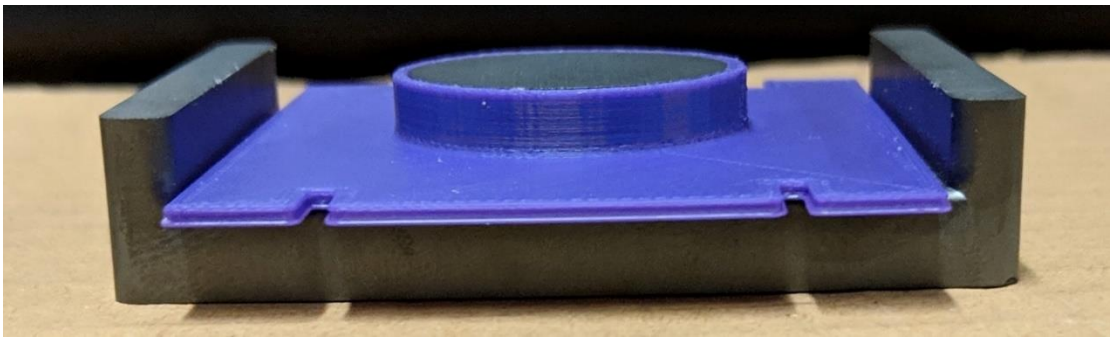

Figure 1.11: Custom Bobbin

Figure 1.12: Bobbin with Separate Primary and Secondary

In 3D printing bobbins, one concern is the automatically generated structures. If a surface in 3D printing overhangs by more than 30 degrees (depending on the printer), then structures are automatically added in the design to prevent uneven surfaces from the print melting. These supports must be removed before winding which opens the opportunity to accidentally fracture the bobbin and possibly have uneven dielectric along the core creating more problems. There were two optimal solutions found. Firstly, the bobbin can be printed in two equal halves and taped together which prints no supports

and an even dielectric gap along the bobbin. Another more expensive solution is to use a specialty printer such as the Stratasys Mojo 3D printer [19] which is able to print the entire bobbin encased in a supporting sphere that can be dissolved after the print leaving an intact entire bobbin.

1.6 Chapter References

[1] B. Singh, B. N. Singh, A. Chandra, K. Al-Haddad, A. Pandey and D. P. Kothari, "A review of single-phase improved power quality AC-DC converters," in *IEEE Transactions on Industrial Electronics*, vol. 50, no. 5, pp. 962-981, Oct. 2003, doi: 10.1109/TIE.2003.817609.

[2] Dranetz-BMI, *Power Quality Analysis*. Edison, New Jersey, USA: Dranetz-BMI:2003.

[3] T. Wildi, *Electrical Machines, Drives and Power Systems*, 6th ed. London, UK: Pearson Education, 2005.

[4] M. Holt, *Mike Holt's Illustrated Guide to Power Quality*. Sunrise, FL: Mike Holt Enterprises, Inc., 2014.

[5] IEEE Recommended Practice and Requirements for Harmonic Control in Electric Power Systems, IEEE Standard 519, 2014.

[6] Electromagnetic compatibility (EMC) - Part 3-2: Limits - Limits for harmonic current emissions (equipment input current ≤16 A per phase), IEC Standard 61000-3-2, 2018.

[7] *Power Factor Correction (PFC) Handbook,* Revision 5, ON Semiconductor, April 2014. Accessed on: October 8, 2019. [Online]. Available: https://www.onsemi.com/pub/Collateral/HBD853-D.PDF.

[8] Texas Instruments. (2017). PFC for Not Dummies. Accessed on: October 8, 2019. [Online]. Available: https://training.ti.com/sites/default/files/docs/HVI_PFC_Not_For_Dummies_Peter_Meaney.pdf

[9] W.G. Hurley and W.H. Wolfle, *Transformers and Inductors for Power Electronics: Theory, Design, and Applications*. West Sussex, UK: John Wiley & Sons Ltd., 2014.

[10] Ferroxcube. "3C90 Material Specification." Ferroxcube. https://www.ferroxcube.com/upload/media/product/file/MDS/3c90.pdf (accessed Oct 8, 2019).

[11] P. L. Dowell, "Effects of eddy currents in transformer windings," in *Proceedings of the Institution of Electrical Engineers*, vol. 113, no. 8, pp. 1387-1394, August 1966. doi: 10.1049/piee.1966.0236.

[12] C. R. Sullivan and R. Y. Zhang, "Simplified design method for litz wire," *2014 IEEE Applied Power Electronics Conference and Exposition - APEC 2014*, Fort Worth, TX, 2014, pp. 2667-2674. doi: 10.1109/APEC.2014.6803681.

[13] J. Mühlethaler, J. Biela, J. W. Kolar and A. Ecklebe, "Improved core loss calculation for magnetic components employed in power electronic system," *2011 Twenty-Sixth Annual IEEE Applied Power Electronics Conference and Exposition (APEC)*, Fort Worth, TX, 2011, pp. 1729-1736. doi: 10.1109/APEC.2011.5744829.

[14] J. Mühlethaler, J. Biela, J. W. Kolar and A. Ecklebe, "Core Losses Under the DC Bias Condition Based on Steinmetz Parameters," in *IEEE Transactions on Power Electronics*, vol. 27, no. 2, pp. 953-963, Feb. 2012. doi: 10.1109/TPEL.2011.2160971.

[15] J. Wang, K. J. Dagan, X. Yuan, W. Wang and P. H. Mellor, "A Practical Approach for Core Loss Estimation of a High-Current Gapped Inductor in PWM Converters With a User-Friendly Loss Map," in *IEEE Transactions on Power Electronics*, vol. 34, no. 6, pp. 5697-5710, June 2019. doi: 10.1109/TPEL.2018.2867264.

[16] O. Garcia, J. A. Cobos, R. Prieto, J. Uceda and S. Ollero, "A standard design method for high frequency PCB transformers," *Proceedings of INTELEC 95. 17th International Telecommunications Energy Conference*, The Hague, Netherlands, 1995, pp. 335-339. doi: 10.1109/INTLEC.1995.498972.

[17] B. Li, Q. Li and F. C. Lee, "A novel PCB winding transformer with controllable leakage integration for a 6.6kW 500kHz high efficiency high density bi-directional on-board charger," *2017 IEEE Applied Power Electronics Conference and Exposition (APEC)*, Tampa, FL, 2017, pp. 2917-2924. doi: 10.1109/APEC.2017.7931111.

[18] Fusion 360. "Self-paced learning for Fusion 360." Autodesk. https://f360ap.autodesk.com/courses (accessed Oct. 8, 2019).

[19] Stratasys. "Stratasys Mojo FDM Specifications." CATI. https://www.cati.com/3d-printing/stratasys-3d-printers/mojo/ (accessed Oct. 8, 2019).

2 PLECS- AND ANSYS-BASED ANALYSIS

2.1 Introduction

As briefly discussed in the Literature Review section, designing magnetic components has many factors ranging from core material, geometry, and size to winding material, type, and sizing which makes selecting the best design difficult. Many pre-existing analytical solutions such as Ansys PExprt, Ansys Maxwell, and Plexim PLECS can provide optimal results, however, complicated designs such as those for PFC applications and resonant converters are less straight-forward. In this section, these pre-existing analytical tools will be discussed and compared.

2.2 Ansys Design Methodology

With the modern Ansys Electronics Desktop application, different Ansys programs can be used and coupled within one project. This enables a standard Ansys workflow for analyzing the various components of an electromagnetic project such as a SMPS converter [20]. In this ideal workflow, the desired circuit is first simulated in Ansys Simplorer with ideal components. Then, using the magnetic component's waveforms, an optimized magnetic design is created in Ansys PExprt. Additionally in PExprt, a Maxwell Finite Element Analysis (FEA) file can be created. Back in Simplorer, this Maxwell FEA file can replace the desired magnetic component so that upon initiating the simulation, the Maxwell file can simultaneously simulate and provide excitations to the Maxwell model. In the following sections, each software tool will be discussed along with its weaknesses.

2.2.1 Ansys PExprt

Ansys PExprt is a magnetic component design software for power electronics applications outside of Electromagnetic Interference (EMI) filtering [21]. Upon opening

PExprt, the user is able to select the magnetic component type (Figure 3.1). The component type chosen determines the following steps but the general workflow remains the same.

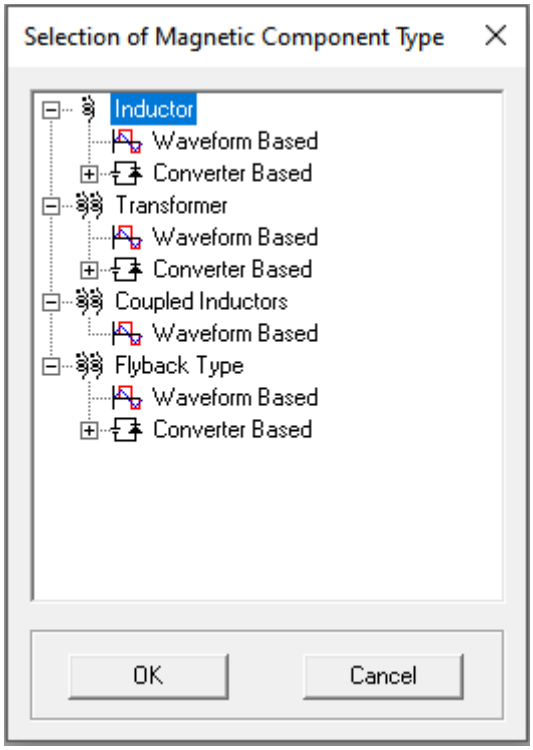

Figure 2.1: PExprt Component Menu

Premade libraries of core dimensions, wire specifications, and materials can be selected to reduce design time or PExprt also allows users to input custom materials and dimensions. If no specific cores or materials are selected, the tool will automatically choose a reasonable range of possible options at runtime.

The first tab (Waveforms) is to input basic design parameters (similar to the standard inductor design process) such as voltage waveform type, component conduction mode, frequency, and desired (minimum) inductance with a window to show the waveform being chosen. In the case of PFC design, these specifications are a little more challenging than data input from a simulation scope. The inductance must be the

minimal value needed to ensure proper operation while the voltage and current should be the maximum conditions to prevent component damage.

The next tab (Design Inputs) focuses on more subjective design objectives (Figure 3.2). In the experimentation done, designing for a gap over both legs allowed usage of a variable height bobbin as previously discussed for quick testing. Another key setting was the maximum flux density (B_{max}) to saturation flux density (B_{sat}) ratio. Since PExprt is not meant for PFC applications, this needs to be set as high as 90% to ensure optimal utilization of the core window.

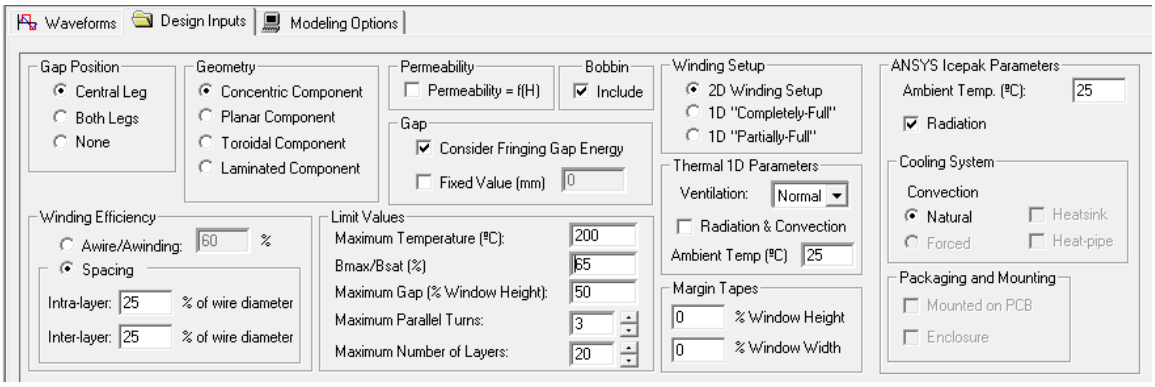

Figure 2.2: PExprt Design Inputs Tab

On the final tab (Modeling Options), the loss modeling and optimization methods can be determined. For basic PFC applications, the loss calculated is incorrect regardless as the loss is calculated for a full cycle of the worst case condition. Additionally, the available core inputs do not require Steinmetz Premagnetization Graphs (SPGs) so the tool is relying on uncorrected i^2GSE which is inaccurate for cores with DC bias as discussed previously.

After running the simulation, the tool sorts various design combinations by best overall with the option for the user to sort by power loss, size, or inductance (for a fixed air gap). By calculating possible options, the tool considers various turns ratios, combinations of parallel turns, and different air gap sizes on top of the different core

material, geometry, and size combinations. The tool even gives a final breakdown of parameters for each core that can be used in deciding possible options (Figures 2.3 and 2.4).

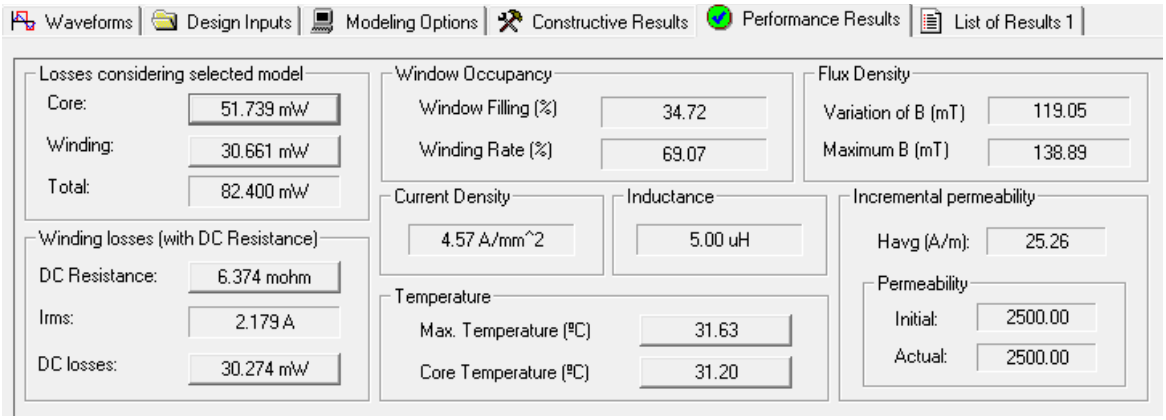

Figure 2.3: PExprt Simulation Results Tab

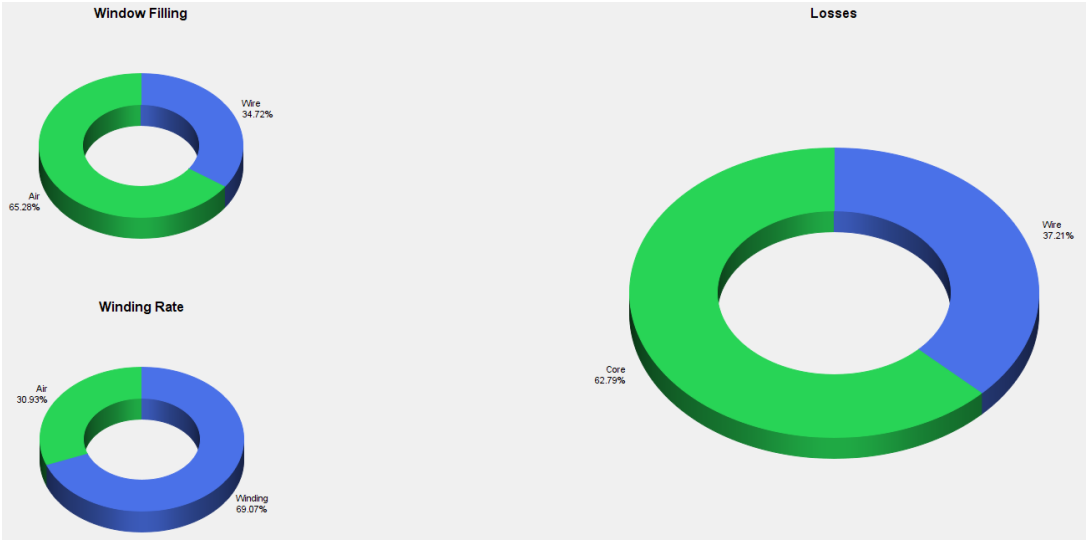

Figure 2.4: PExprt Loss Breakdown

After a design has been selected, it can be imported into the PEmag [22] module and have the winding arrangement physically modeled (Figure 3.5). Once the windings are satisfactorily arranged, PEmag can create an Ansys FEA simulation file automatically with the basic material properties included.

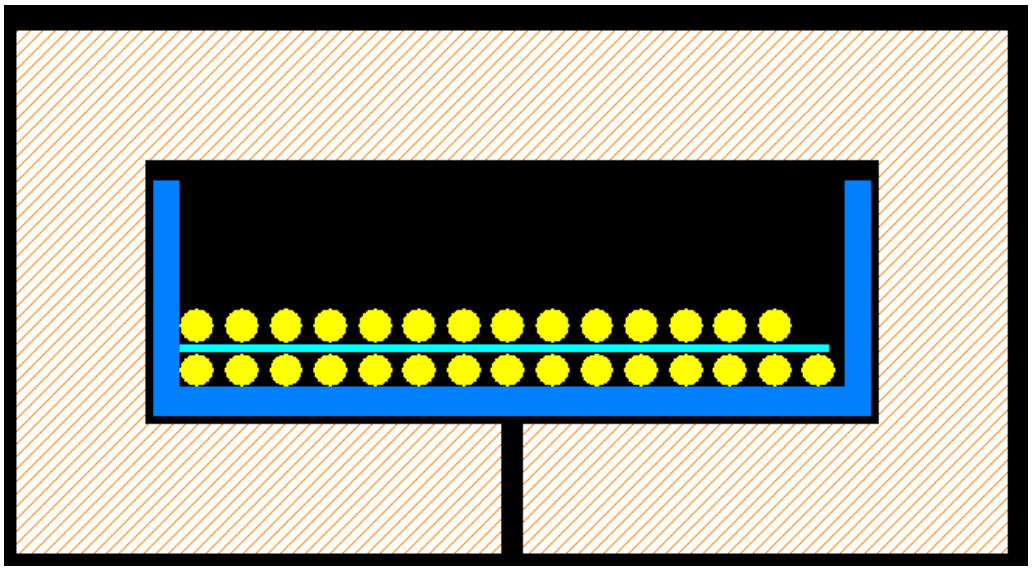

Figure 2.5: PEmag Winding Construction

For the practical engineer wishing to get more out of his or her magnetic components, Ansys PExprt is a great tool with adequate documentation. The tool loses its value under a few specific cases. Firstly, PFC designs require finesse and several iterations to get practical designs since the optimization is fundamentally based on a flawed loss calculation. Additionally, converter topologies that rely on leakage inductance (such as certain resonant converters) require another design process to achieve desired results. PExprt has no calculation for resonant inductance and the hand calculation is a rough approximation. FEA is the best method to determine leakage inductance without physically measuring the component. If PEmag were used for resonant magnetic component design, each design (core material/geometry/size and winding combination) would have to be run through a FEA simulation and modified based on the estimated leakage. Finally, the FEA generated model through PExprt's PEmag tool is a sufficient starting point but requires work as will also be discussed in the next section.

2.2.2 Ansys Maxwell

Ansys Maxwell is a Finite Element Analysis (FEA) tool in the Ansys Electronics Desktop package that analyzes models in the lower frequency range i.e. below megahertz (MHz) [23]. HFSS, another application in the Ansys Electronics package, is a similar FEA tool that models higher frequency models from the megahertz (MHz) to gigahertz (GHz) range [23] hence it can be used for power electronics EMI analysis which is outside of the scope for this thesis. Primary applications of Ansys Maxwell include modeling electromagnetic components such as electric machines, power transformers, wireless charging units, and power electronics components. Ansys Maxwell has a considerable learning curve so [24] was referenced frequently in addition to the documentation ([23]).

From a design in PExprt, a Maxwell model can be automatically generated using PExprt's complementary tool, PEmag. This Maxwell model can be seen below wound with solid wire on two center-gapped E-cores (Figures 2.6 and 2.7). The model's geometry is accurate to the core specifications from PExprt but this model is only useful for the defined single DC-DC period unless modifications are made to the model.

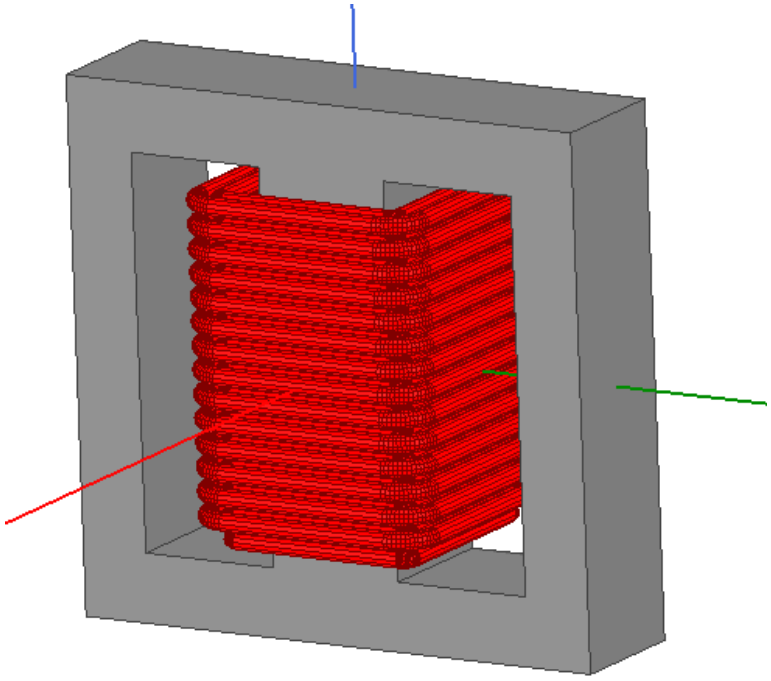

Figure 2.6: Maxwell Complete FEA Model

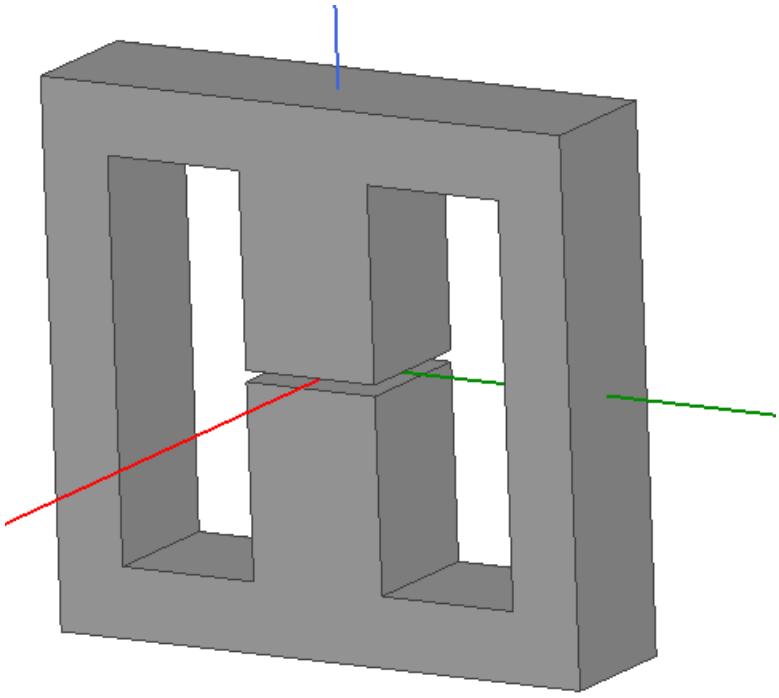

Figure 2.7: Maxwell FEA Core Model

Firstly, the windings are generated similarly to the PEmag construction which is straight around the core and not connected together. This is a good winding approximation since the signal will near instantly propagate through the wire but creates additional simulation burden since the signal must be applied and simulated in each winding. With this in mind, multiple windings are helpful for examining eddy current effects through simulation but, ultimately, the core only sees the Ampere-turn product from the windings as a whole. When running a Magnetic Transient simulation (discussed later in detail), it was found that replacing the discrete windings with one cylindrical winding model that received the same excitation was successful for core excitation but not winding analysis. Figure 2.8 demonstrates a 2D coupled inductor with idealized primary and secondary windings and air gap.

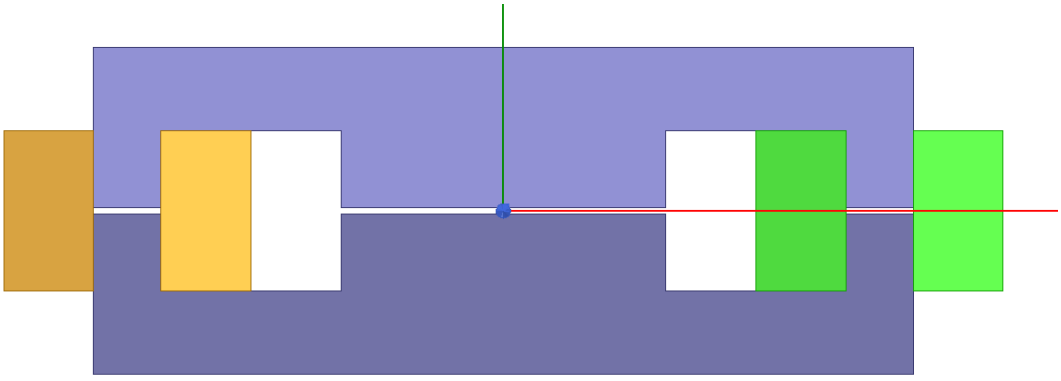

Figure 2.8: Maxwell Idealized Winding Planar Transformer

Moving onto the materials, PEmag creates a new material for each winding of parallel windings (i.e. CondMat1_1) and gives an oversimplified characterization of the magnetic material (called CoreMat). For simplicity, it is easier to convert all windings into one copper material with the same properties. For the core, more changes must be done. In the default CoreMat material (Figure 2.9), no core loss model is setup and a

linear permeability is given from the PExprt material properties. By specifying a nonlinear relative permeability in Maxwell, a B-H curve can be edited to give a more realistic core with saturation effects (Figure 2.10). However, this contains many challenges of its own. A major problem here is the curve must begin at zero and be monotonically increasing for Maxwell to accept the custom B-H curve (see figure). To overcome this, a premagnetization curve is needed which can be interpolated from a measured B-H curve which adds the possibility for more error.

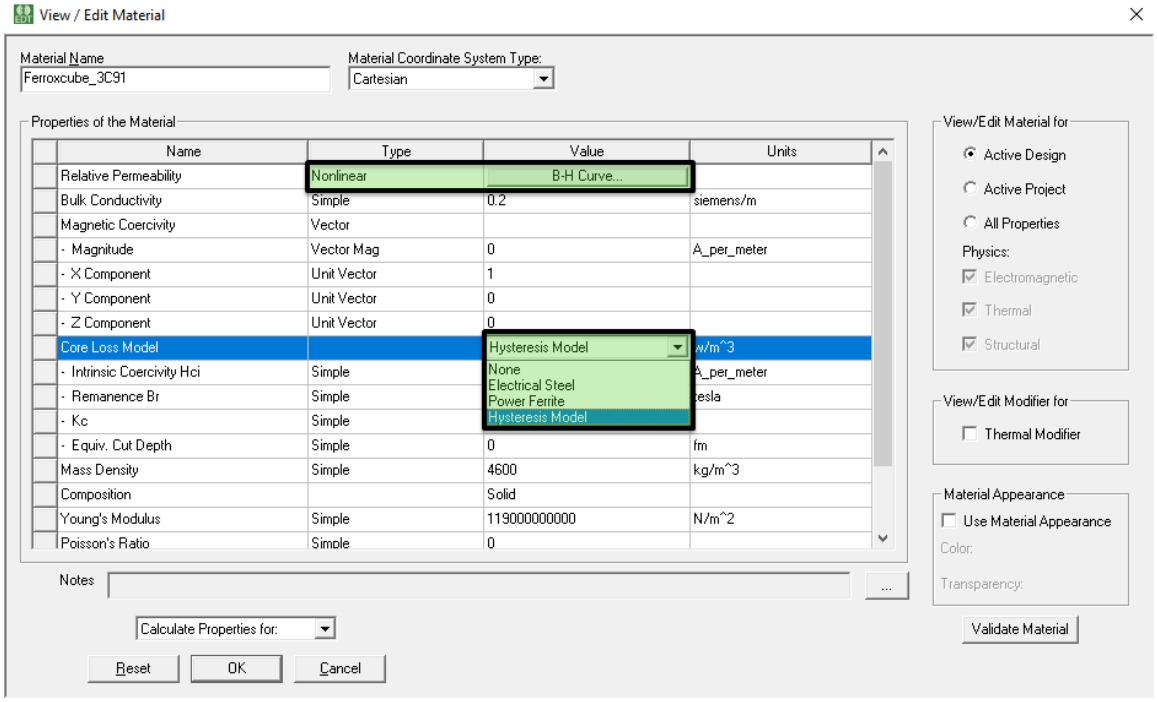

Figure 2.9: Maxwell Material Properties

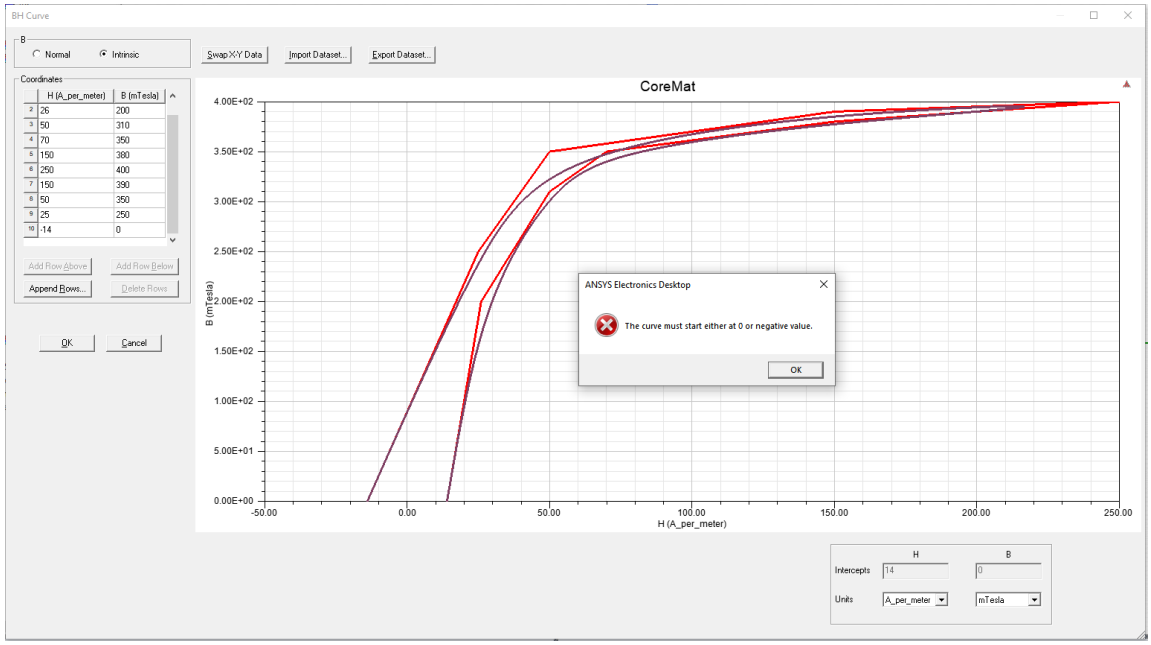

Figure 2.10: Maxwell Material B-H Error

It is not until runtime that the discrete winding types become problematic. As previously mentioned, the discrete windings are useful for Magnetic Eddy Current simulations but make a Magnetic Transient simulation nearly impossible to run. For background, there are three magnetic simulation types (Figure 2.11): Magnetostatic, Eddy Current, and Transient. Eddy Current simulations are most useful for determining the best winding structure through providing the actual period-long excitation but all material must be simple (i.e. linear) for this simulation type. On the other hand, Magnetostatic simulations are designed for looking at the material without analyzing eddy effects since the excitation provided is a static bias point (worst-case condition of the provided period). Finally, Transient simulations combine these two simulation types at the largest computational burden with a dynamic excitation waveform.

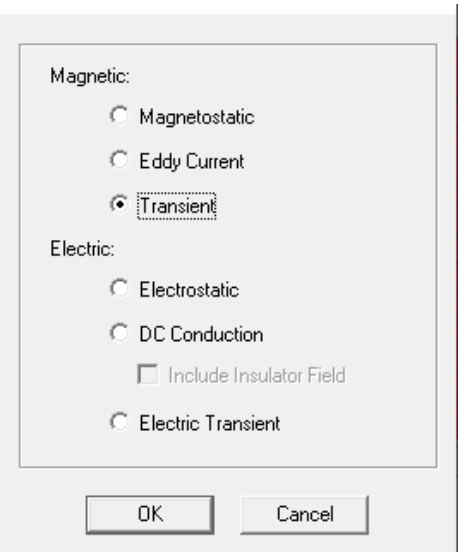

Figure 2.11: Maxwell Simulation Types

In Finite Element Analysis, the most difficult part is the trade-off between speed and accuracy. Many factors influence this (including the winding model) but the most important is the mesh size. The mesh is a grid covering the model where Maxwell's equations are physically calculated within each cube. By specifying a finer or tighter mesh, the accuracy will improve at the cost of computational burden. In Maxwell, it is possible to import an optimized (adaptive) mesh by running the same model in another simulation type (i.e. Magnetostatic) which will improve the simulation time and accuracy. An optimized mesh using this procedure can be seen in Figure 2.12. Another factor affecting this trade-off is dimensionality. 2D simulations run faster than 3D simulations but can neglect some critical aspects such as leakage inductances that lead to major losses in practicality.

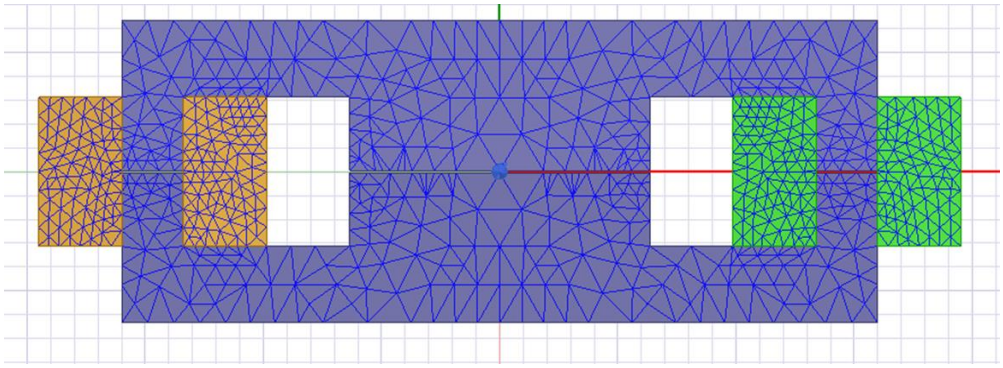

Figure 2.12: Maxwell Optimized Mesh

Now that the model has proper material properties and model settings, a simulation can be run to determine the model's key parameters (the purpose of using Ansys Maxwell). First in the material properties, basic Steinmetz coefficients can be specified which still has the same problems discussed in the Literature Review. Before running a simulation in which inductance values are desired, the Maxwell Design Settings need to be updated to compute either the apparent or incremental inductance matrix (Figure 2.13). Leakage inductance and magnetizing inductance can simply be found after running the simulation by plotting the inductance between the input and output ports. In the case of a transformer, leakage inductance can be found by the inductance matrix from primary to secondary windings.

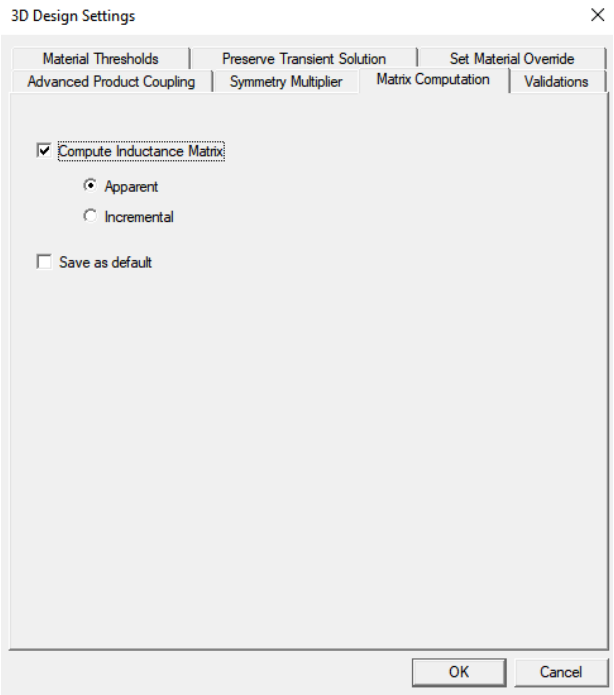

Figure 2.13: Maxwell Inductance Design Setting

2.2.3 Ansys Maxwell Cosimulation

In the previous section, many aspects of FEA simulations with Ansys Maxwell were discussed. As mentioned, the simulation type dictates the possible excitation with Transient simulations being the most accepting of waveform inputs. Ansys Maxwell has three possible options for creating custom switching excitations as opposed to simply providing a repeating formula (i.e. Sine): Ansys Maxwell Circuit Editor, Mathworks Simulink, and Ansys Simplorer. In previous versions of Ansys Maxwell, the major cosimulation tool was Ansys Maxwell's circuit editor. With Ansys Electronics Desktop, cosimulations are possible with Ansys' more powerful SPICE simulator Ansys Simplorer. Despite this being a critical component of the Ansys workflow as discussed previously, Ansys Simplorer and Ansys Maxwell require some workarounds in order to work.

A requirement of Ansys is that for a cosimulation to take place, the Maxwell model must involve motion similar to an electric machine. This is a simple fix that was

overcome by turning the outer simulation boundary into a rotational motion field with zero initial motion. The Simplorer model then commands a motion into the Maxwell model so these ports were grounded in Simplorer's motion domain. Besides several other minor settings, the simulation began. Initially, a 3D Maxwell simulation was used that resulted in the computer crashing due to high levels of memory access both from the complicated circuit simulation and the full-wave FEA simulation. Increasing time step did not result in a faster simulation as the Maxwell model was the limiting factor. Furthermore, loosening the mesh helped increase simulation time slightly but still was slow. Finally, converting the model to 2D with the various model changes discussed in the prior section allowed the simulation to run for an entire sine wave cycle. All FEA tools (including Ansys) are extremely memory intensive. Because of this, it is recommended that 3D FEA simulations are used exclusively for model validation rather than design purposes as confirmed in [25]. The results of a Simplorer-Maxwell cosimulation example are discussed in the Results section.

2.3 Plexim PLECS

Besides the Ansys cosimulation, combinations of cores, air gaps, and turns can be directly tested in Plexim PLECS circuit simulator's magnetics domain [26]. PLECS is able to model these components better than the standard coupled inductor modeling method through usage of the capacitance-permeance model [27]. The PLECS magnetics model can be used by simply replacing an ideal magnetic component with a custom magnetic path. As can be seen below (Figure 2.14), windings are placed on the magnetic circuit (while following dot convention) with a hysteretic core. The core has basic parameters such as effective area (A_e), flux path length (l_e), coercive magnetic field strength (H_c), and saturation magnetic flux density (B_{sat}) which are enough to define a basic hysteresis loop (Figure 2.15).

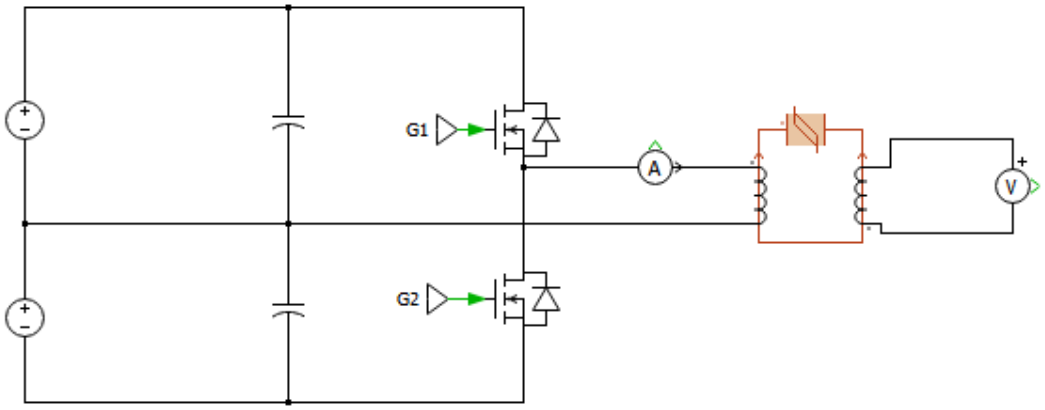

Figure 2.14: PLECS Magnetics Domain Schematic

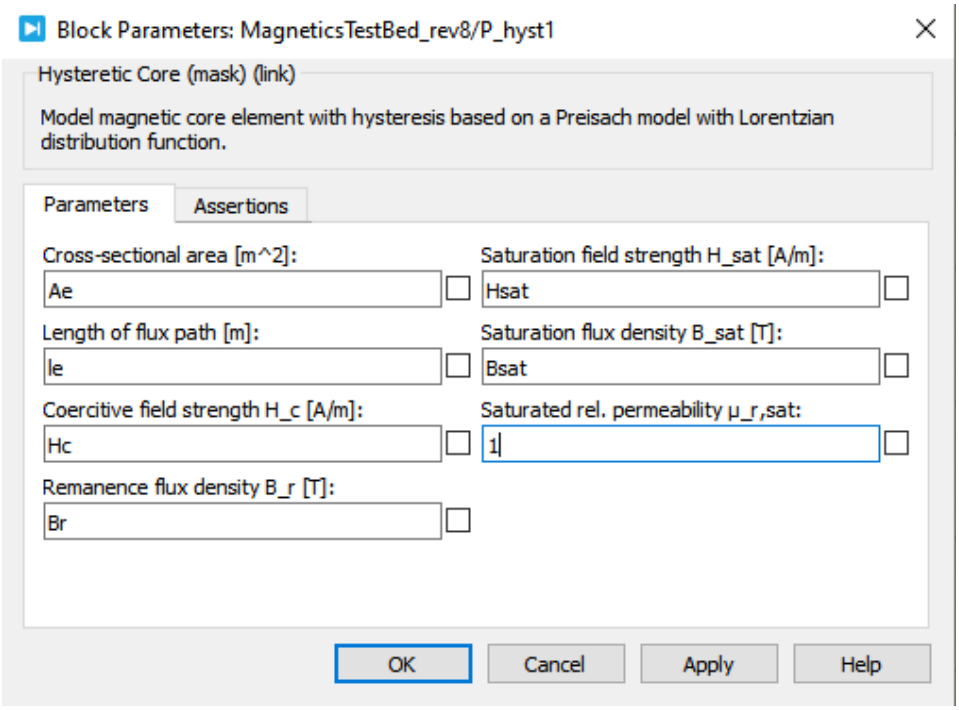

Figure 2.15: PLECS Magnetics Domain Core Settings

2.4 Chapter References

[20] Z. Tang, M. Christini, T. Koga, “Wireless Power Transfer Using Maxwell and Simplorer,” presented at the 2012 Automotive Simulation World Congress, Detroit, Michigan, USA, Oct. 30–31, 2012.

[21] *Power Electronics Expert (PExprt™) Manual*. (2018). Ansys. Accessed: Oct. 9, 2019. [Online]. Available: https://www.ansys.com/

[22] *Power Electronics Magnetics (PEmag™) Manual*. (2018). Ansys. Accessed: Oct. 9, 2019. [Online]. Available: https://www.ansys.com/

[23] *ANSYS Electronics 19.2 Manual*. (2018). Ansys. Accessed: Oct. 9, 2019. [Online]. Available: https://www.ansys.com/

[24] Kamyar K, Canada. Ansys Maxwell. Accessed: Oct. 9, 2019. [Online Video]. Available: https://www.youtube.com/channel/UCGfupEFC34BNIqKlCGUKwEA/

[25] C. R. Sullivan, High-Frequency Magnetics Design: Overview and winding Loss. Accessed on: October 9, 2019. [online] Available: http://www.psma.com/sites/default/files/uploads/tech-forums-magnetics/presentations/high-frequency-magnetics-design-overview-and-winding-loss.pdf.

[26] *Plecs User Manual*. (Version 4.3), Plexim. Accessed: Oct. 9, 2019. [Online]. Available: https://www.plexim.com/sites/default/files/plecsmanual.pdf

[27] J. Allmeling, W. Hammer and J. Schönberger, "Transient simulation of magnetic circuits using the permeance-capacitance analogy," *2012 IEEE 13th Workshop on Control and Modeling for Power Electronics (COMPEL)*, Kyoto, 2012, pp. 1-6. doi: 10.1109/COMPEL.2012.6251786.

3 MAGNETICS TEST BED

3.1 Concept Validation

Despite this magnetics test bed method having been published as discussed in the Literature Review, it still needs to be validated in simulation and hardware. For the purposes of this thesis, the approach can be generalized in two parts. The first stage is the loss map generation using hardware and post-processing tools as seen in Figure 3.1. The second stage is the data query where the generated loss maps are integrated with a circuit simulation tool (Figure 3.2).

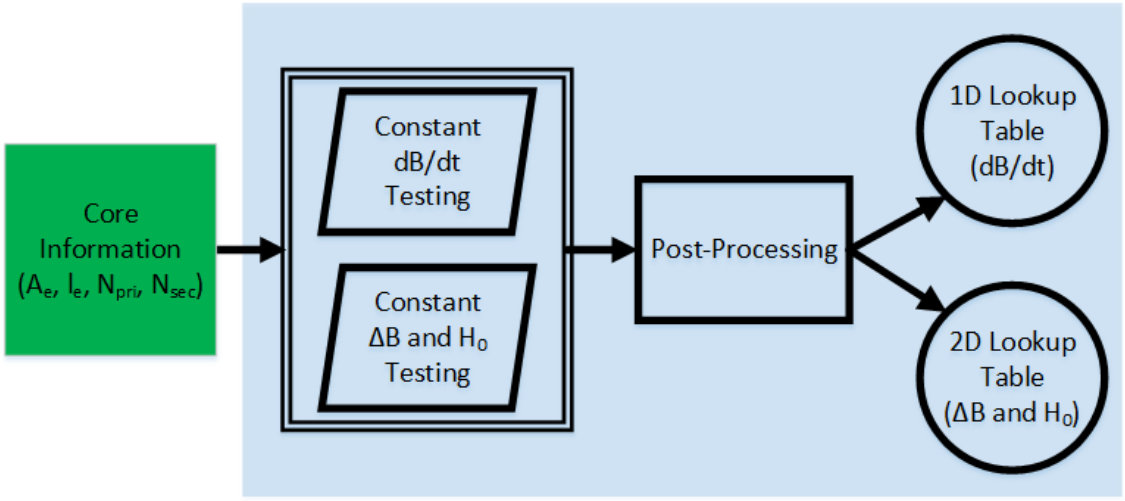

Figure 3.1: Magnetics Test Bed Loss Map Generation Flowchart

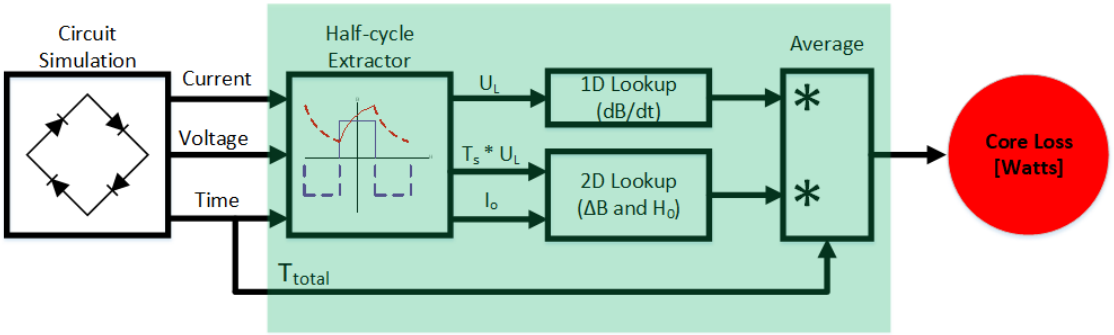

Figure 3.2: Magnetics Test Bed Data Query Flowchart

3.1.1 PLECS Magnetics Test Bed

The process outlined by Figures 3.1 and 3.2 was firstly implemented in PLECS using Python Scripting. Figure 3.3 demonstrates the magnetics test bed using PLECS' magnetics domain for a core with hysteresis as well as the key measurements to be recorded ($I_{primary}$ and $V_{secondary}$). Figure 3.4 is a basic implementation of the triple pulse test control scheme needed. The signal path starts with a PWM (Pulse Width Modulation) generator followed by a delay block to hold the first pulse for a duration of T_{mag}. The PWM signals then flow for two more cycles before the PWM signal is switched to zero at calculated time $T_{demagnetize}$. After half of a switching cycle, the PWM signal has both channels set to zero at T_{stop}. This triple pulse test implementation signal is shown in Figure 3.5.

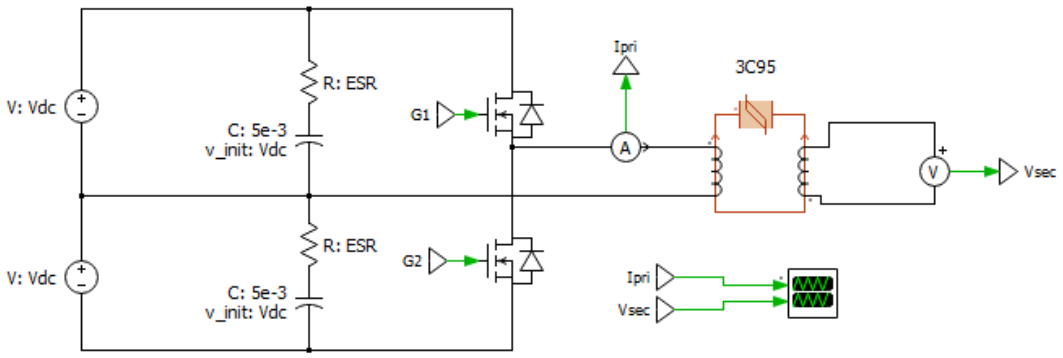

Figure 3.3: PLECS Magnetics Test Bed - Power Stage

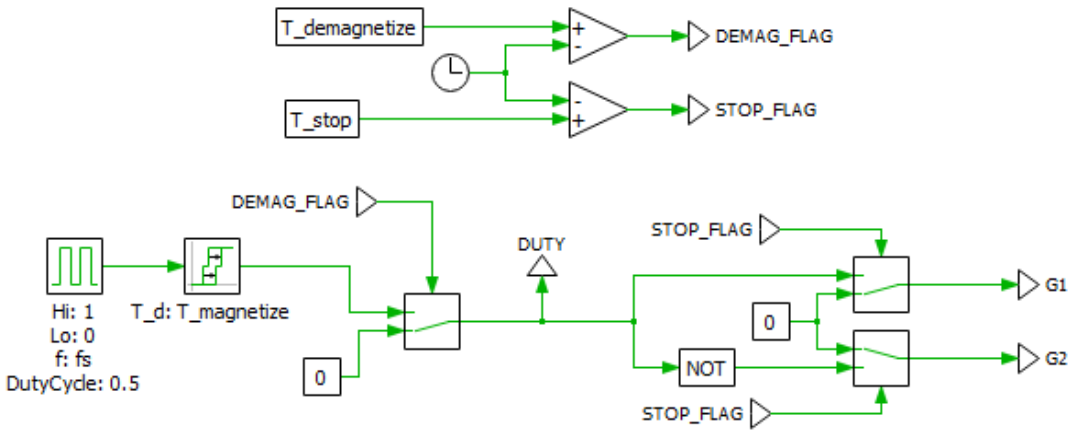

Figure 3.4: PLECS Magnetics Test Bed - Control Stage

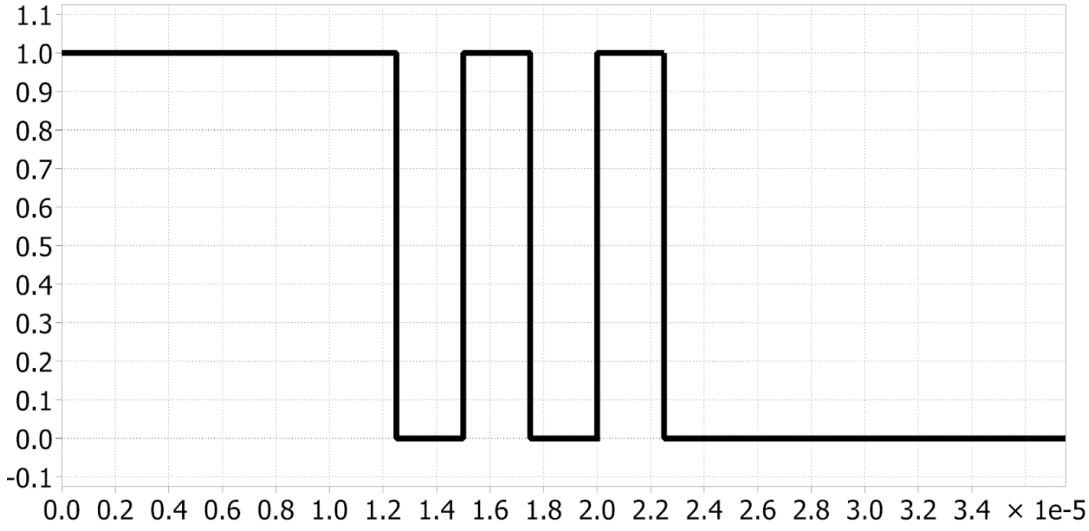

Figure 3.5: PLECS Magnetics Test Bed - PWM Signal

With the hardware setup and PWM signal successfully established in simulation, the resulting plot of secondary voltage and primary current versus time forms the basis for calculation and is shown in Figure 3.6. In these simulations, nonidealities are to be expected. The primary measured current can become extremely high due to several factors. Firstly, the voltage sources used are ideal and will provide any current needed in order to maintain their voltage setpoint. Next, the PLECS magnetic domain model is

fairly complicated with many simulation nonidealities that can lead to a core consuming copious amounts of current.

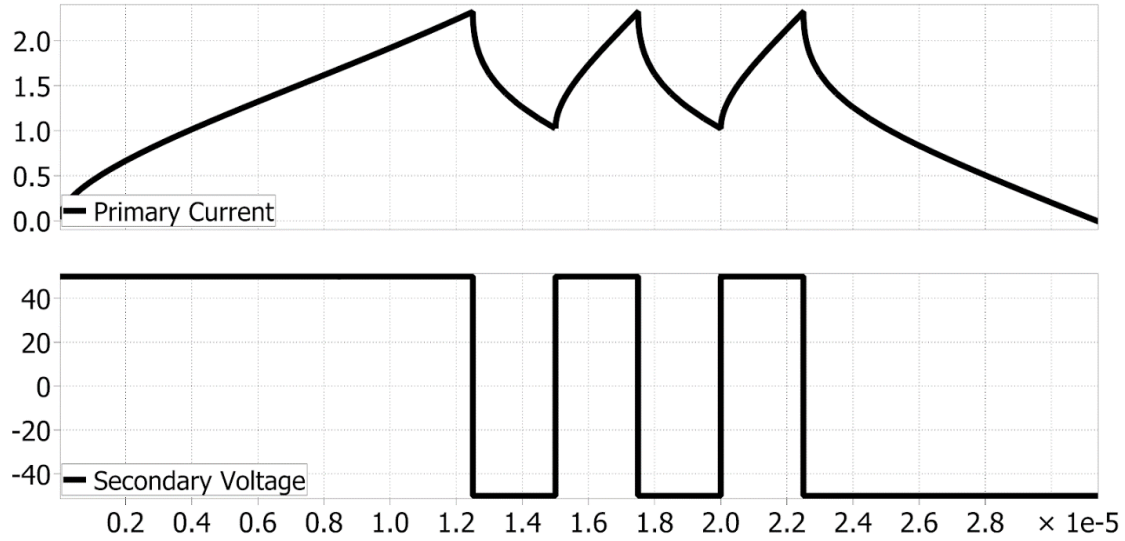

Figure 3.6: PLECS Magnetics Test Bed - Output Signals

The results shown in Figure 3.6 are representative of one test. To generate the maps, many individual tests are run belonging to one of two groups: constant dB/dt and constant ΔB, H_o. For tests to have a constant dB/dt, the voltage sources will remain at a constant voltage (V_{DC}) since this quantity is directly proportional to dB/dt while the switching frequency and magnetization time will be varied. Likewise, tests in the constant ΔB, H_o category will have a fixed magnetization time (for H_o) and a fixed V_{DC}/T_s ratio (for ΔB). This means the constant ΔB, H_o tests will vary the voltage and switching frequency such that the switching frequency and voltage increase together.

To test the procedure and construct a preliminary loss map, the PLECS circuit was scripted using the XML Python interface [26]. Through this scripting, a filename was passed to the simulation for renaming results and saving to different folders for the two tests. Next, voltages, magnetization times, and switching frequencies were passed

through the XML interface and the circuit was simulated. This procedure provided enough data for initial validation of the loss map and MATLAB post-processing.

In designing the tests, the first step is finding starting and ending points for the voltages, frequencies, and magnetization times. The voltages and frequencies are simply selected based on the material's optimal ranges from the data sheet as well as including possible operation range from the desired circuit. Magnetization time is not as directly related since the system current is related to the capacitance, inductance, and parasitics resulting in a nonlinear LC oscillating current. One method to have a better grasp is interpolating magnetization time versus current to ensure a better trend in the final stages.

3.2 MATLAB Post-processing

After running the two sets of tests containing many individual tests each, post-processing can begin to extract key parameters from each test before creating a trend of the values. Referring back to Figures 3.1 and 3.2, the data firstly needs to be processed in a loss map generation script that outputs two saved map files. With these saved map files, the loss map query script will be able to query the two loss maps using time, current, and voltage waveforms recorded using a circuit simulation's inductor.

3.2.1 MATLAB Loss Map Generation

One critical program used in the loss map generation is the Parameter Extractor function. This function intakes the circuit waveforms (time, current, voltage), number of turns (N_{pri} and N_{sec}), effective area (A_e), and effective path length (l_e) before boiling the circuit waveforms down into four critical parameters: energy loss (ΔQ), change in magnetic flux density (ΔB), slope of magnetic flux density (dB/dt), and magnetic field intensity bias (H_o). Firstly, these results can be used to ensure ΔB, H_o, and dB/dt

remained constant in their respective tests. If one of the parameters strayed from the constant value, it becomes easier to preventively remove the data point or collect it again and preserve the map's accuracy. Secondly, since the loss map only depends on these parameters, not the waveforms, this function has more flexibility in obtaining the parameters which becomes beneficial once hardware is involved where noise and LC oscillations become prevalent.

The Parameter Extractor works by firstly breaking the signal into intervals based on the first highest |dV/dt| which indicates the voltage transitioning from a high-level pulse to a low-level pulse. Since the wave patterns of voltage and current are already known due to the standard triple pulse test form, special fit types are applied to the input signals to extract key circuit quantities such as switching frequency, magnetization time, maximum DC voltage, and average current bias. Afterwards, only the steady-state interval is considered and parameters extracted from this portion will be returned for future function usage.

With these critical parameters returned, the loss maps can be finally generated. The first step is removing tests with a saturated core which can be determined based on the calculated steady-state hysteresis curve parameters. Afterwards, the data is simply interpolated into two maps using the specific test data. As previously mentioned, the 1D map with constant ΔB and H_o returns a scaling factor. This scaling factor is determined by normalizing the loss values to the voltage that was used for the constant dB/dt testing. Finally, the two loss maps are saved for use in the loss map query.

3.2.2 MATLAB Loss Map Query

Like the loss map generation, the first stage is a Half-cycle Extractor that operates similarly to the Parameter Extractor with the main exception being that the

Half-cycle Extractor returns circuit parameters (T_s, V_{dc}, I_o) and not magnetic parameters. In computation, a major difference between the two is that the half-cycle extractor only works with simulation so noise-processing is not required and zero-crossings of the voltage waveform can be used to break the waveform into a stream of half-cycle parameters.

With the half-cycle parameters, the program firstly runs a lookup using the tables. Next, the outputs corresponding to each half-cycle set are multiplied together to give a scaled energy loss that is divided by cycle time to give half-cycle power loss. Finally, all of the scaled power losses are averaged (using the total simulation time).

3.3 Hardware Implementation

With the concept proven successfully in simulation, it is time to work on a hardware implementation. For the hardware test rig, key tasks were combining equipment for forming the physical setup and designing the microcontroller code since the MATLAB processing code was already created and validated in the simulation tests. Through hardware testing, an unexpected difficulty arose from noise and oscillations in the waves which resulted in modifying the parameter extraction file since the noise only affected the one step.

3.3.1 Physical Equipment

The overall hardware setup is shown in Figure 3.7. Tables 3.1 and 3.2 outline the components used in the construction of this test bed along with Appendix A containing the board layout used in the custom half-bridge circuit used. For the purposes of this section, a Ferroxcube P36/22-3C91 ungapped core was used with 7:7 turns of 18 AWG enameled magnet wire. Additionally, in the original magnetics test bed paper ([15]),

IGBTs (Insulated-gate Bipolar Transistors) were used which limited the possible frequency and voltage range while this thesis utilized SiCFETs (Silicon Carbide Field Effect Transistors).

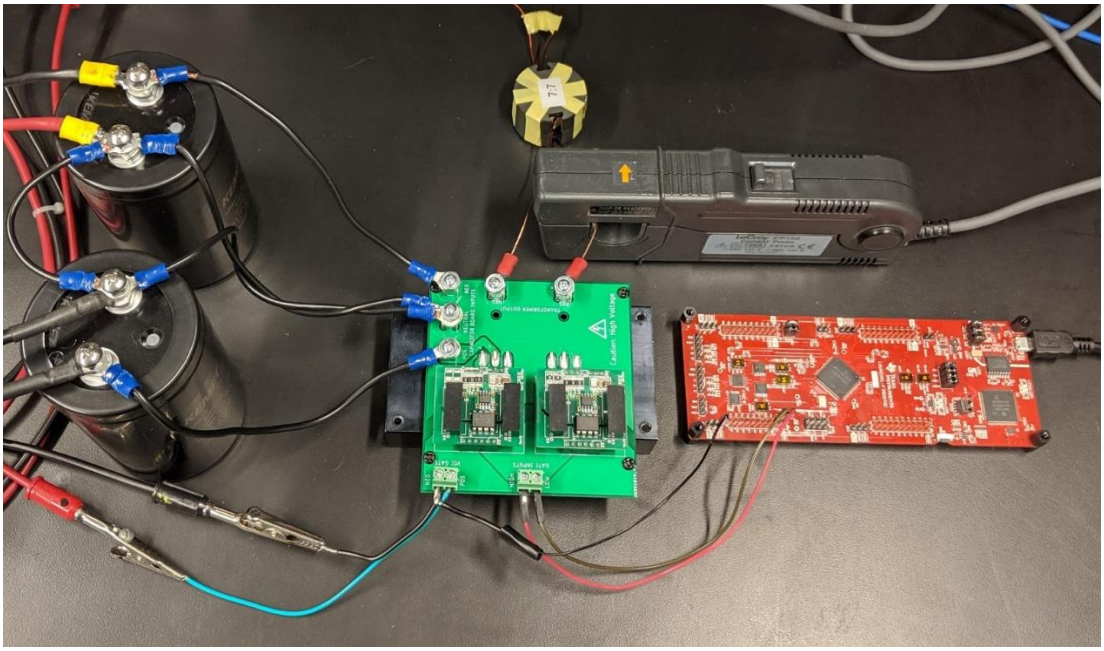

Figure 3.7: Magnetics Test Bed Hardware Implementation

Table 3.1: Magnetics Test Bed Measurement Equipment

Test Equipment	
Low-Power DC Source	1 x BK Precision DC Power Supply (30V/3A)
High-Power DC Sources	2 x Controllable Magna Power (V_O > 200V)
Oscilloscope	1 x LeCroy Waverunner 6200A
Voltage Probe	1 x LeCroy ADP305
Current Probe	1 x LeCroy CP150

Table 3.2: Magnetics Test Bed Equipment Half Bridge

Half-Bridge Circuit	
Microcontroller	1 x TI LAUNCHXL-F280049C
DC Link Capacitors	Kemet ALS70A332MF500 (500V 3.3mF)
Printed Computer Board (PCB)	1 x Custom - see [Appendix A]
SiCFET	2 x CREE C2M0025120D
Single SiCFET Gate Driver	2 x CREE CRD-001
Gate Driver Mounting Connectors	2 x Sullins 6-position 0.1" Gold Connector 4 x Sullins 3-position 0.1" Gold Connector
Metal Mounting Blocks	5 x Wurth 6-Pin M3 Power Terminal
Miscellaneous	Heatsink, Plastic M3 terminals, Ring Terminals

3.3.2 Microcontroller software

One of the benefits of this B-H extraction technique is the triple pulse test as discussed in the Literature Review. Using the triple pulse test allows equipment with lower ratings to be used since the large currents are transient and do not require continuous ratings. Unfortunately, this creates difficulty in coding as the PWM signal is custom which means the microcontroller's code cannot simply take advantage of the TI ePWM module [28]. Ultimately, a simple code using the TI F280049C's GPIO registers along with short delays through the assembly nop command and longer delys using the DELAY_US function [28] as can be seen in Appendix B. One critical factor in the proper execution of this program is changing the Code Composer Studio (CCS) compilation settings to maximize optimization levels with a priority on execution speed (not memory) across the global program.

In the course of this thesis, an automated code generator was implemented using Simulink's ePWM block with various trip register commands (see Figure 3.8) [29] [30]. Unfortunately, this method took significantly longer to generate the code as compared to the simple CCS handwritten code. Additionally, Simulink would occasionally throw an error if the code simulation running in external mode was terminated before the simulation hit its fixed end time which varied run-by-run.

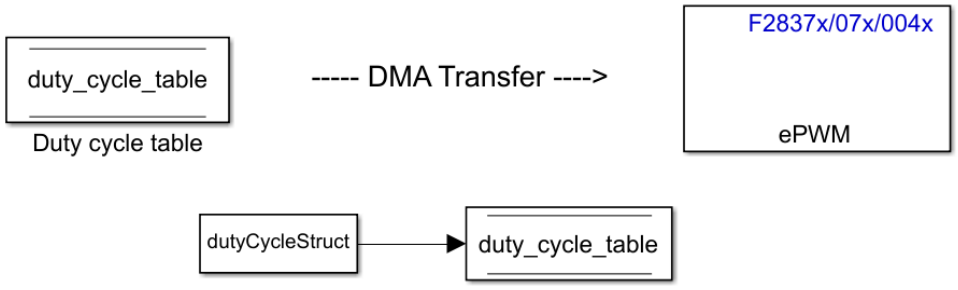

Figure 3.8: Simulink Automated F280049C ePWM

3.3.3 Single Test Results

After running one test, the LeCroy oscilloscope results can be seen in Figure 3.9. These results are similar to the idealized results with more noise and oscillations along the waveform. Upon importing the data to MATLAB Figures 3.10 and 3.11 show a closer view of how much noise the signal contains.

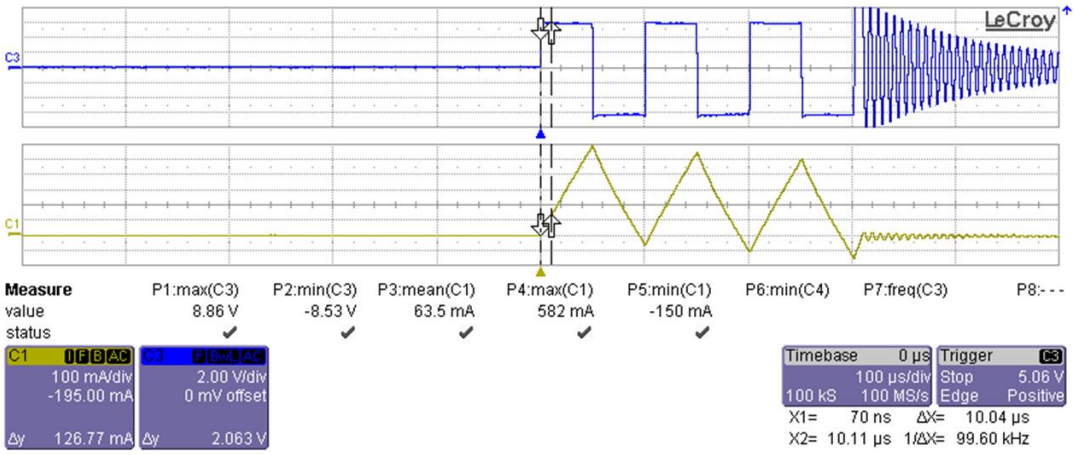

Figure 3.9: Single Magnetics Test Bed Results

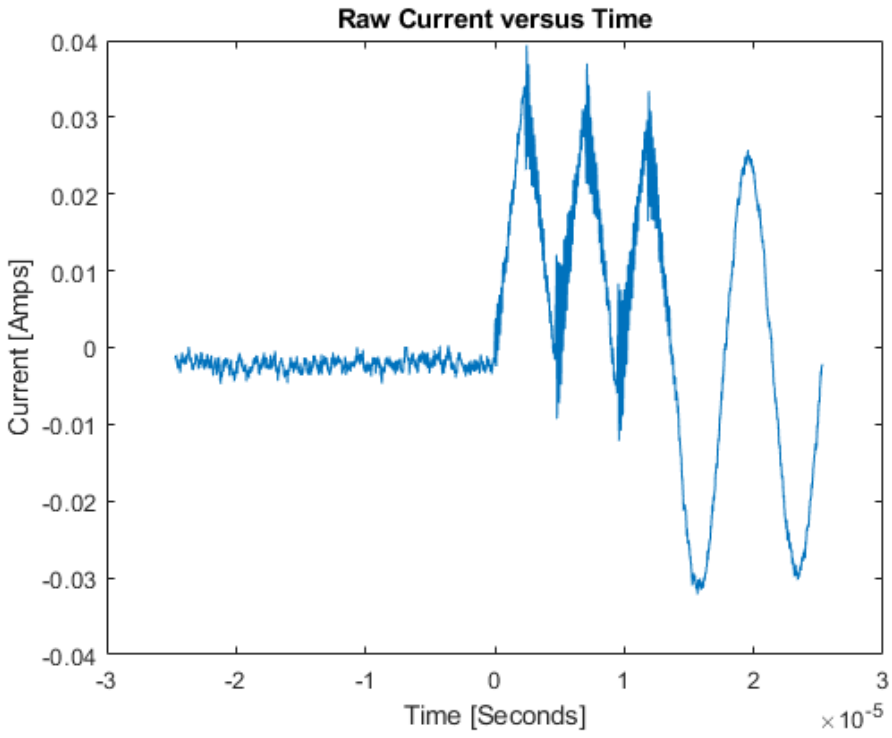

Figure 3.10: Raw Current Waveform

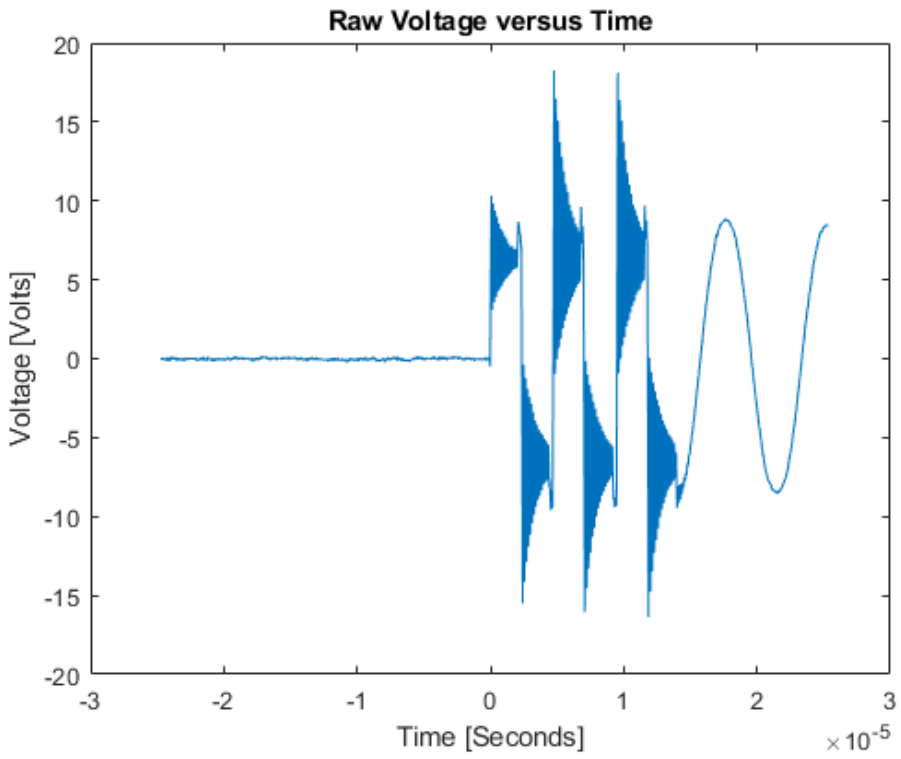

Figure 3.11: Raw Voltage Waveform

After some basic filtering and reconstruction of the signals to most closely represent their ideal states, the input signals are overlaid in Figure 3.12. One thing to note is the sequence of cycles. The first cycle's purpose is to establish a DC bias through the magnetization current, the second cycle is designed to stabilize the BH loop, and the final cycle is the desired steady-state cycle that will be used for data analysis. Since the third cycle is the most desired, it is critical to ensure at least the steady-state cycle has clear results in the oscilloscope whereas the magnetizing cycle can have more noise (even after post-processing) but will not affect the results significantly. At this point, the circuit processing works much like the simulation portion by extracting key parameters then using the key parameters to draw trends about the core loss.

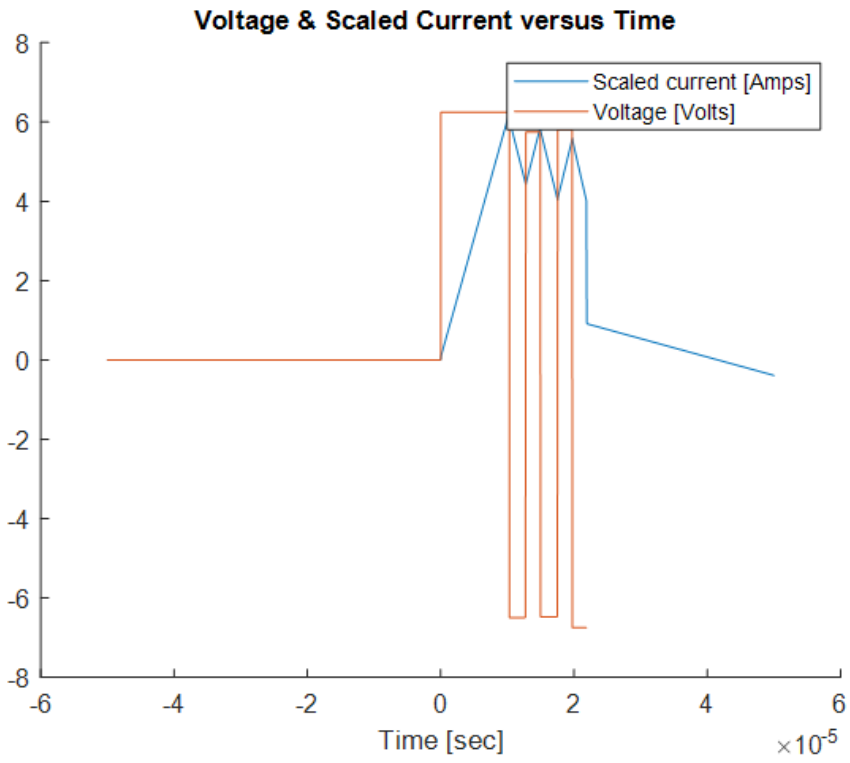

Figure 3.12: Filtered Input Waveforms

3.3.4 Sample Core Characterization

Using the testing procedure established with the simulation procedure along with the waveform cleaning and hardware test bed, it becomes possible to finish the core loss characterization of a Ferroxcube P36/22-3C91 core [31][32] as can be seen in Figures 3.13 and 3.14. These plots were generated by inputting the test points found in Tables 3.3 and 3.4 into the microcontroller code (see Appendix B) where T_S is the switching period and equivalent to the inverse of the switching frequency. T_{mag} is the magnetization period length which has been previously discussed.

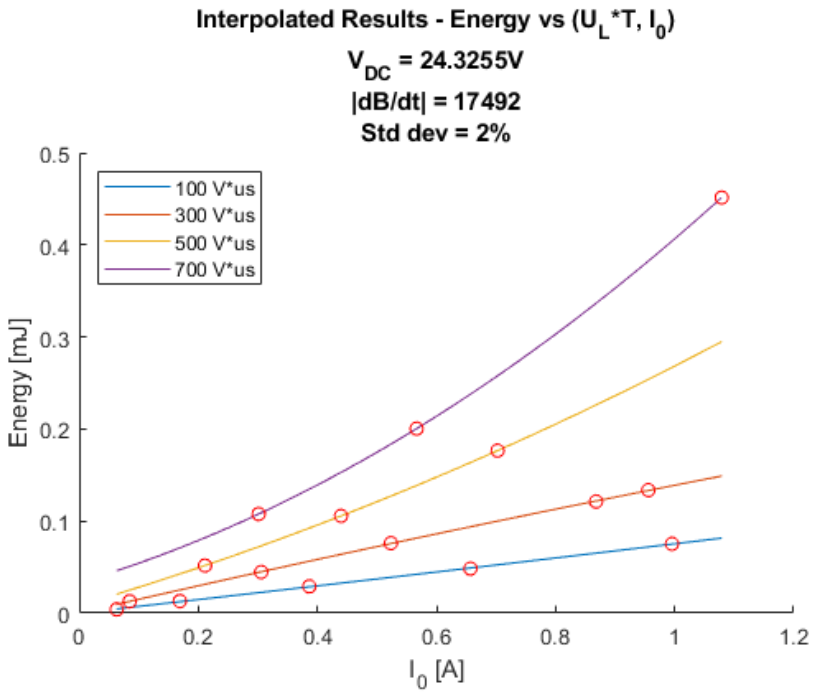

*Figure 3.13: Magnetic Core Loss Map - Energy versus (U_L*T_s, I_o)*

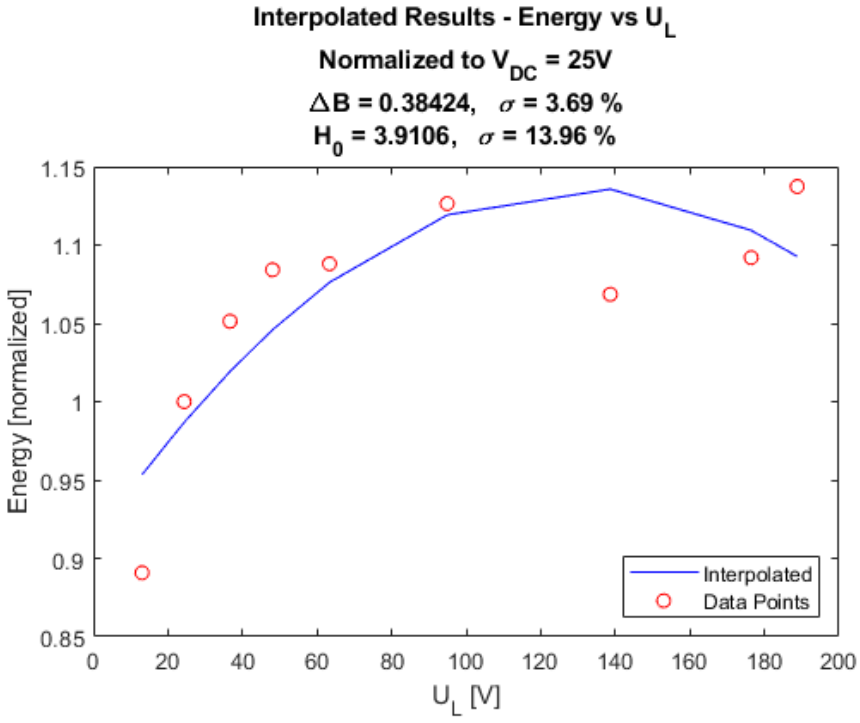

Figure 3.14: Magnetic Core Loss Map - Energy versus U_L

Table 3.3: Constant dB/dt Test Points with Constant VDC (VDC+ = 20 V, VDC- = 21.2 V)

T_s [µs]	T_{mag} [µs]
5	2.5, 5, 10, 15, 20, 25, 26, 27, 28
10	5, 10, 15, 20, 21, 25, 26, 27, 28
20	10, 15, 20, 25, 26, 27, 28
30	15, 20, 25, 26, 27, 28, 29

Table 3.4: Constant (ΔB, Io) Test Points with Constant Tmag (Tmag = Ts/2)

V_{DC}^+ [V]	T_s [µs]
10	80
20	40
30	26.6
40	20
53	15
80	10
120	6.6
150	5.3
160	5

One caveat with the magnetization period is that it cannot be less than T_{on} which is the duration of ON time; in the case of this magnetics test bed, duty cycle is fixed at one half so $T_{on} = T_s/2$. If T_{mag} is less than T_{on}, then a negative DC bias is created which does not aid the interpolation efforts. Additionally, in Table 3.4, only V_{DC}^+ is listed since V_{DC}^- was chosen to be the variable supply for ensuring $V_L^- = V_L^+$, a condition that requires testing iteration to accomplish.

Finally, not all of the points tested were used in the loss map for a few reasons. The primary reason is core saturation. In the loss map data presented here (Figures 3.13 and 3.14), saturation data was not included since the loss significantly increases resulting in a lesser curve fit. With that said, this magnetics loss map is helpful in determining the material's exact saturation magnetic flux density (B_{sat}) if the material were unknown.

3.4 Chapter References

[28] Texas Instruments. *TMS320F28004x Microcontrollers Technical Reference Manual*. (2019). [Online]. Accessed: Oct. 17, 2019. Available: http://www.ti.com/lit/ug/sprui33c/sprui33c.pdf.

[29] MathWorks. *C280x/C2802x/C2803x/C2805x/C2806x/C2833x/C2834x/F28M3x/F2807x/F2837xD/F2837xS/F2838x/F28004x ePWM*. [Online]. Accessed: Oct. 17, 2019. Available: https://www.mathworks.com/help/supportpkg/texasinstrumentsc2000/ref/c280xc2802xc2803xc2805xc2806xc2833xc2834xf28m3xf2807xf2837xdf2837xsf2838xf28004xepwm.html.

[30] MathWorks. *Modify Duty Cycle of ePWM Using DMA*. [Online]. Accessed: Oct. 17, 2019. Available: https://www.mathworks.com/help/supportpkg/texasinstrumentsc2000/ug/modify-epwm-using-dma.html

[31] Ferroxcube. *P36/22 Core Product Specifications*. [Online]. Accessed: Oct. 18, 2019. Available: https://www.ferroxcube.com/upload/media/product/file/Pr_ds/P36_22.pdf

[32] Ferroxcube. *3C91 Material Product Specifications*. [Online]. Accessed: Oct. 18, 2019. Available: https://www.ferroxcube.com/upload/media/product/file/MDS/3c91.pdf

4 RESULTS

4.1 Ansys Cosimulation

Through running a cosimulation with an inductor designed using Ansys PExprt and hand-modeled with linear magnetic materials in 2D Ansys Maxwell, the below figures demonstrate the results obtained for a resonant coupled inductor design after running for a week on a computer running Windows 10 with i7-4770, 16Gb RAM (Random Access Memory), and 1Tb HDD (Hard Disk Drive). Since this simulation was massively memory intensive, many accuracy reductions (i.e. 2D, looser mesh, winding abstraction) led to results being less accurate than intended. The Magnetostatic analysis and Eddy Current analysis proved to be more useful as they require fewer resources to run.

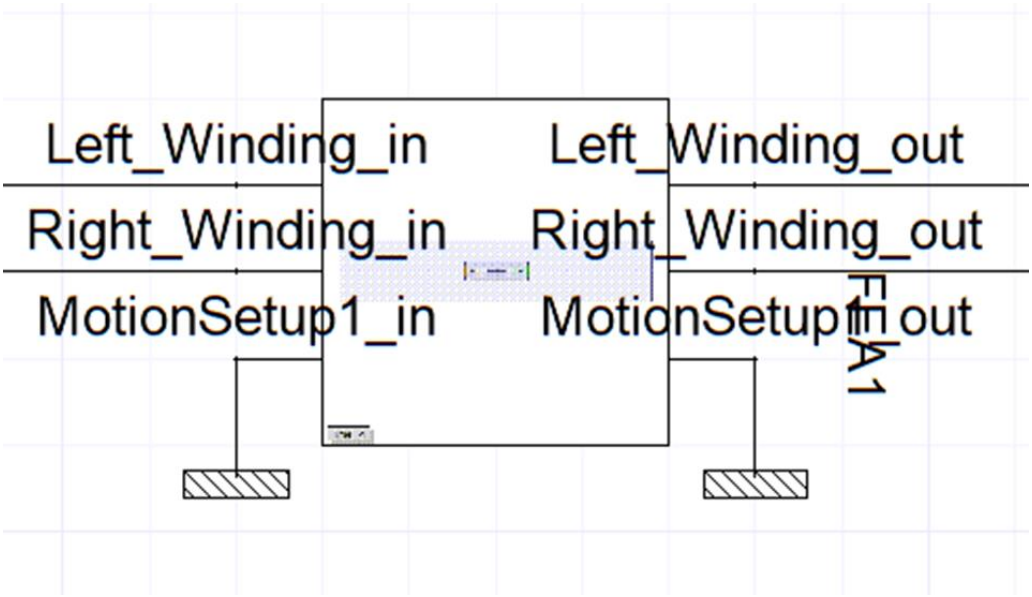

Figure 4.1: Simplorer Cosimulation Block for Maxwell Model

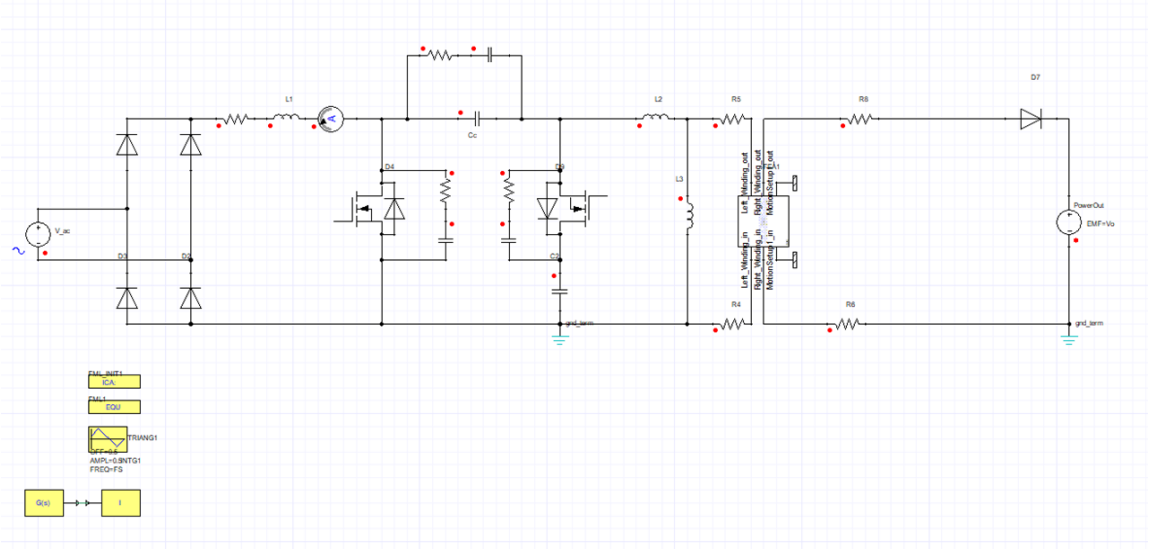

Figure 4.2: Cosimulation Simplorer Schematic

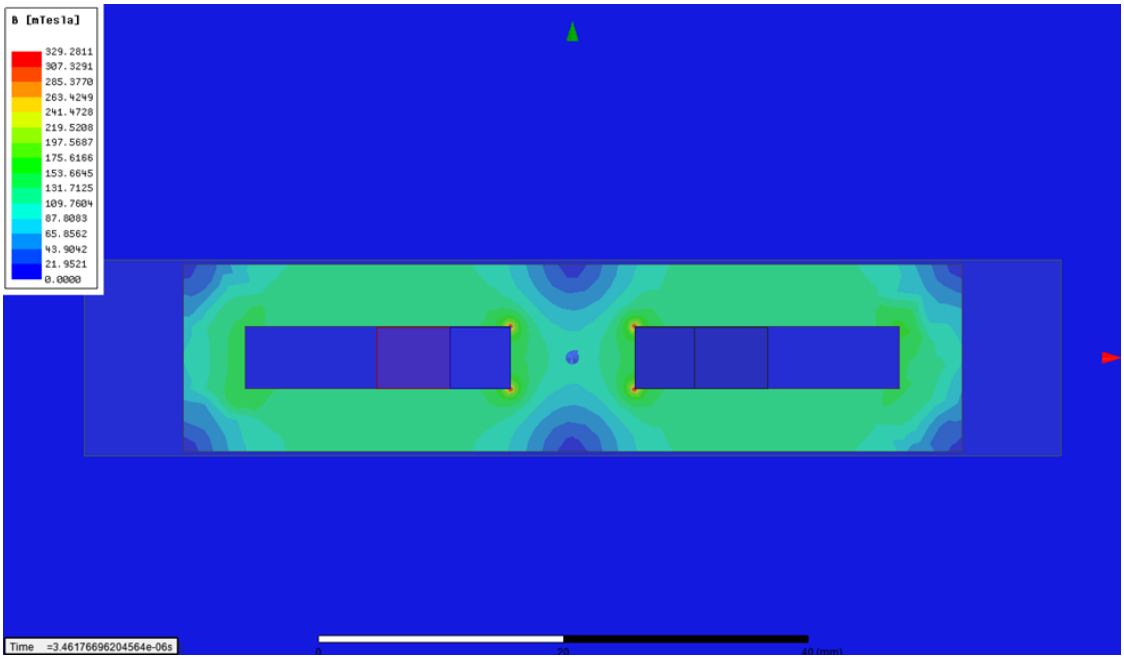

Figure 4.3: Ansys Maxwell Magnetic Flux Density of Core

4.2 Magnetics Test Bed

In order to validate the magnetics test bed, a basic sinusoidal circuit setup was used since this setup type is traditionally used in determining Steinmetz parameters and

serves as a good standard as shown in Figure 4.4 with 100V for V_{max} and 200 kHz for f_s. Figure 4.5 shows the excitation (current and voltage) waveforms captured.

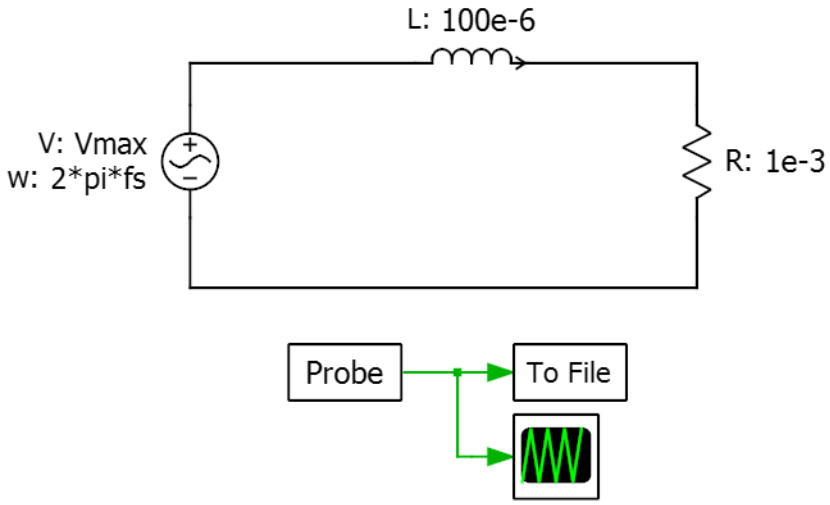

Figure 4.4: Sinusoidal Excitation Circuit for Magnetics Test Bed Validation

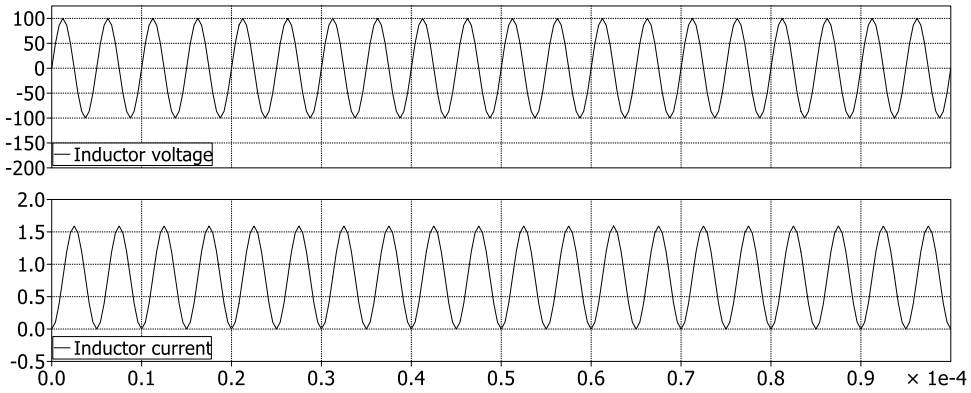

Figure 4.5: Sinusoidal Excitation Waveforms for Magnetics Test Bed Validation

After using the sinusoidal circuit's excitations with the circuit post-processing functionality of the magnetics test bed procedure, a plot of the energy loss (per cycle) versus switching period is shown in Figure 4.6. Through further calculation, the power equivalent loss of this circuit was found to be 1.9452 Watts.

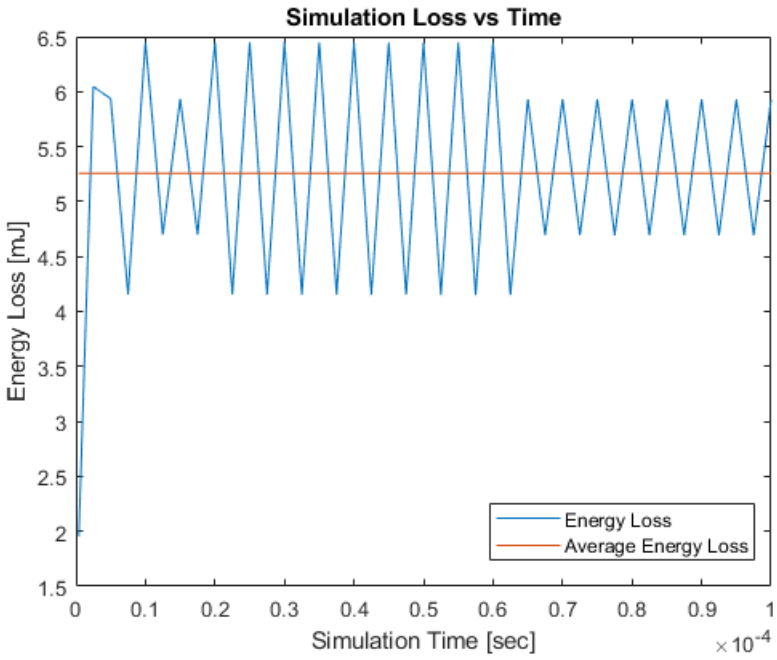

Figure 4.6: Magnetics Test Bed Energy Loss versus Switching Cycle

In order to validate the core loss number, the Ferroxcube Soft Ferrite Design Tool (SFDT) [33] was used to find the core loss density at 25˚C (room temperature) as shown in Figure 4.7. By multiplying the loss density found in Figure 4.7 with the Ferroxcube P36/22-3C91 core volume of 10,700 mm^3 [31], the ideal core loss was found to be 2.2 Watts. This means that the loss calculated using the magnetics test bed contained 11.6% error for this case with no DC bias and a core with no air gap.

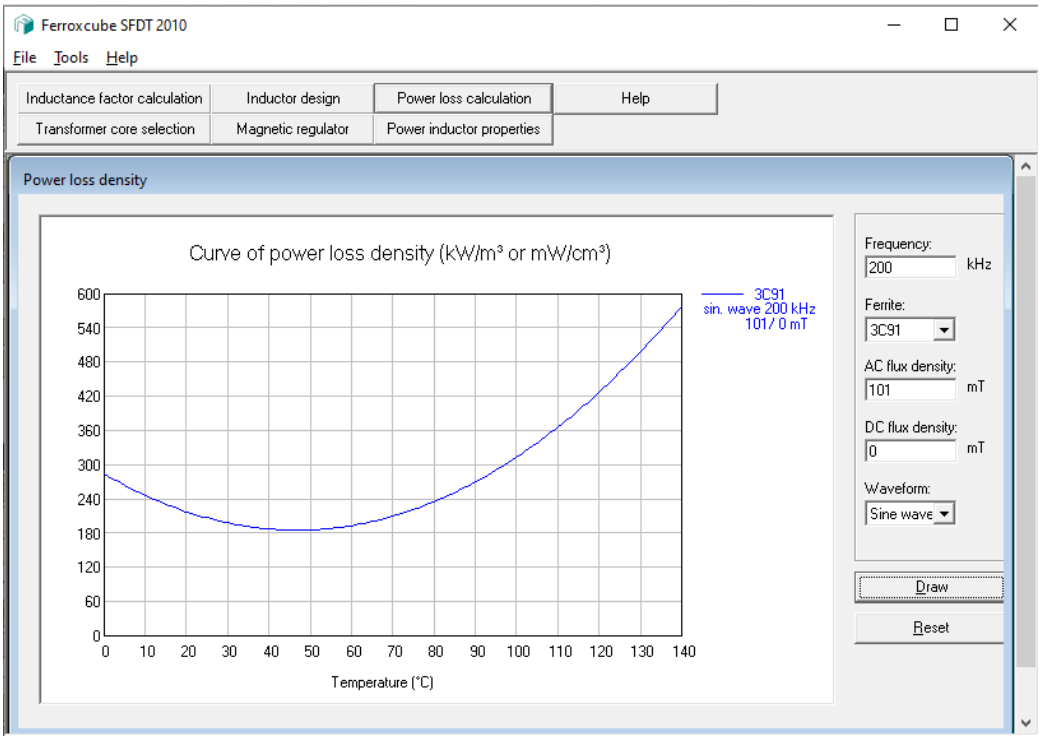

Figure 4.7: Magnetics Test Bed Loss Verification using SFDT

4.3 Chapter References

[33] Ferroxcube. Design Tool. [Online]. Accessed: Oct. 28, 2019. Available: https://www.ferroxcube.com/en-global/design_tool/index

5 CONCLUSIONS & FUTURE WORK

5.1 PLECS- and Ansys-based Analysis

Standard analytical tools are exceptional at their main purpose: quickly designing and optimizing DC-DC inductors and transformers. However, PFC presents its own challenge. As shown, each tool had pros and cons when applied to PFC but most were able to be useful with the specific procedures discussed previously and summarized below.

5.1.1 Ansys PExprt

Ansys PExprt was used successfully to quickly design magnetic cores for DC-DC but still had shortcomings. Despite not being able to design for PFC applications, PExprt is still useful to design based on worst-case conditions which can be used as a starting point in PFC magnetics design. Additionally, the PExprt Maxwell models were a starting point for Maxwell design.

5.1.2 Ansys Maxwell

Ansys Maxwell was shown to have many merits yet the computational power available over the course of this thesis was insufficient to accurately calculate all needed quantities over the entire switching cycle. For Maxwell to be used properly, it should only be used for design validation in Magnetostatic mode to determine peak parameters (inductances, saturation) and Eddy Current mode to compare winding strategies.

5.1.3 Ansys Simplorer Cosimulation

As mentioned above, the Ansys Simplorer Cosimulation was barely possible and highly impractical. Ansys PExprt and Maxwell are superior tools for validating designs but the cosimulation's resource demand is not worth the results that could be more

quickly and affordable obtained through other means such as a Magnetostatic simulation with the Magnetics Test Bed to determine core loss and Dowell's equation for winding loss.

5.2 Magnetics Test Bed

The Magnetics Test Bed was shown in the results section to be successful and work properly, however, there is still room for improvement and more possible applications. A primary area of improvement is the microcontroller automation. As discussed, hand code was created to effectively implement the triple pulse test but automatic microcontroller code generation and flashing still requires more work. Additionally, the results of this thesis were focused primarily on power factor correction filtering inductors but leakage coupled inductors which can be used in PFC resonant converters equally can benefit from this paper's results using a similar procedure.

5.3 Final Remarks

Overall, the many distinct parts of this project can be formed into one cohesive proposed design procedure for PFC Inductors. Firstly, an ideal circuit simulation is needed to determine required specifications (frequency, minimum magnetizing/leakage inductance) as well as to define the current and voltage waveforms. These specifications are then used to generate several possible designs for the worst case conditions in a design package such as Ansys PExprt. With several completed designs, Ansys Maxwell's Magnetostatic simulation can be used to validate the cores do not saturate as well as meet minimum inductance specifications. With the designs completed, optimization can begin.

In hardware, the magnetics test bed can be used with a custom bobbin to define the core loss given the air gap. With several specific core-air gap combinations, the loss

of each core can be found in circuit simulation. Based on the specified major design objective (size or efficiency), various winding configurations can be analyzed using the existing Ansys Maxwell model in an Eddy Current simulation.

REFERENCES

[1] B. Singh, B. N. Singh, A. Chandra, K. Al-Haddad, A. Pandey and D. P. Kothari, "A review of single-phase improved power quality AC-DC converters," in *IEEE Transactions on Industrial Electronics*, vol. 50, no. 5, pp. 962-981, Oct. 2003, doi: 10.1109/TIE.2003.817609.

[2] Dranetz-BMI, *Power Quality Analysis*. Edison, New Jersey, USA: Dranetz-BMI:2003.

[3] T. Wildi, *Electrical Machines, Drives and Power Systems*, 6th ed. London, UK: Pearson Education, 2005.

[4] M. Holt, *Mike Holt's Illustrated Guide to Power Quality*. Sunrise, FL: Mike Holt Enterprises, Inc., 2014.

[5] IEEE Recommended Practice and Requirements for Harmonic Control in Electric Power Systems, IEEE Standard 519, 2014.

[6] Electromagnetic compatibility (EMC) - Part 3-2: Limits - Limits for harmonic current emissions (equipment input current ≤16 A per phase), IEC Standard 61000-3-2, 2018.

[7] *Power Factor Correction (PFC) Handbook,* Revision 5, ON Semiconductor, April 2014. Accessed on: October 8, 2019. [Online]. Available: https://www.onsemi.com/pub/Collateral/HBD853-D.PDF.

[8] Texas Instruments. (2017). PFC for Not Dummies. Accessed on: October 8, 2019. [Online]. Available: https://training.ti.com/sites/default/files/docs/HVI_PFC_Not_For_Dummies_Peter_Meaney.pdf

[9] W.G. Hurley and W.H. Wolfle, *Transformers and Inductors for Power Electronics: Theory, Design, and Applications*. West Sussex, UK: John Wiley & Sons Ltd., 2014.

[10] Ferroxcube. "3C90 Material Specification." Ferroxcube. https://www.ferroxcube.com/upload/media/product/file/MDS/3c90.pdf (accessed Oct 8, 2019).

[11] C. R. Sullivan and R. Y. Zhang, "Simplified design method for litz wire," *2014 IEEE Applied Power Electronics Conference and Exposition - APEC 2014*, Fort Worth, TX, 2014, pp. 2667-2674. doi: 10.1109/APEC.2014.6803681.

[12] P. L. Dowell, "Effects of eddy currents in transformer windings," in *Proceedings of the Institution of Electrical Engineers*, vol. 113, no. 8, pp. 1387-1394, August 1966. doi: 10.1049/piee.1966.0236.

[13] J. Mühlethaler, J. Biela, J. W. Kolar and A. Ecklebe, "Improved core loss calculation for magnetic components employed in power electronic system," *2011 Twenty-Sixth Annual IEEE Applied Power Electronics Conference and Exposition (APEC)*, Fort Worth, TX, 2011, pp. 1729-1736. doi: 10.1109/APEC.2011.5744829.

[14] J. Mühlethaler, J. Biela, J. W. Kolar and A. Ecklebe, "Core Losses Under the DC Bias Condition Based on Steinmetz Parameters," in *IEEE Transactions on Power Electronics*, vol. 27, no. 2, pp. 953-963, Feb. 2012. doi: 10.1109/TPEL.2011.2160971.

[15] J. Wang, K. J. Dagan, X. Yuan, W. Wang and P. H. Mellor, "A Practical Approach for Core Loss Estimation of a High-Current Gapped Inductor in PWM Converters With a User-Friendly Loss Map," in *IEEE Transactions on Power Electronics*, vol. 34, no. 6, pp. 5697-5710, June 2019. doi: 10.1109/TPEL.2018.2867264.

[16] O. Garcia, J. A. Cobos, R. Prieto, J. Uceda and S. Ollero, "A standard design method for high frequency PCB transformers," *Proceedings of INTELEC 95. 17th International Telecommunications Energy Conference*, The Hague, Netherlands, 1995, pp. 335-339. doi: 10.1109/INTLEC.1995.498972.

[17] B. Li, Q. Li and F. C. Lee, "A novel PCB winding transformer with controllable leakage integration for a 6.6kW 500kHz high efficiency high density bi-directional on-board charger," *2017 IEEE Applied Power Electronics Conference and Exposition (APEC)*, Tampa, FL, 2017, pp. 2917-2924. doi: 10.1109/APEC.2017.7931111.

[18] *Fusion 360 Manual*. (2018). Autodesk. Accessed: Oct. 8, 2019. [Online]. Available: https://f360ap.autodesk.com/courses

[19] Stratasys. "Stratasys Mojo FDM Specifications." CATI. https://www.cati.com/3d-printing/stratasys-3d-printers/mojo/ (accessed Oct. 8, 2019).

[20] Z. Tang, M. Christini, T. Koga, “Wireless Power Transfer Using Maxwell and Simplorer,” presented at the 2012 Automotive Simulation World Congress, Detroit, Michigan, USA, Oct. 30–31, 2012.

[21] *Power Electronics Expert (PExprt™) Manual*. (2018). Ansys. Accessed: Oct. 9, 2019. [Online]. Available: https://www.ansys.com/

[22] *Power Electronics Magnetics (PEmag™) Manual*. (2018). Ansys. Accessed: Oct. 9, 2019. [Online]. Available: https://www.ansys.com/

[23] *ANSYS Electronics 19.2 Manual*. (2018). Ansys. Accessed: Oct. 9, 2019. [Online]. Available: https://www.ansys.com/

[24] Kamyar K, Canada. Ansys Maxwell. Accessed: Oct. 9, 2019. [Online Video]. Available: https://www.youtube.com/channel/UCGfupEFC34BNIqKlCGUKwEA/

[25] C. R. Sullivan, High-Frequency Magnetics Design: Overview and winding Loss. Accessed on: October 9, 2019. [online] Available: http://www.psma.com/sites/default/files/uploads/tech-forums-magnetics/presentations/high-frequency-magnetics-design-overview-and-winding-loss.pdf.

[26] *Plecs User Manual*. (Version 4.3), Plexim. Accessed: Oct. 9, 2019. [Online]. Available: https://www.plexim.com/sites/default/files/plecsmanual.pdf

[27] J. Allmeling, W. Hammer and J. Schönberger, "Transient simulation of magnetic circuits using the permeance-capacitance analogy," *2012 IEEE 13th Workshop on Control and Modeling for Power Electronics (COMPEL)*, Kyoto, 2012, pp. 1-6. doi: 10.1109/COMPEL.2012.6251786.

[28] Texas Instruments. *TMS320F28004x Microcontrollers Technical Reference Manual*. (2019). [Online]. Accessed: Oct. 17, 2019. Available: http://www.ti.com/lit/ug/sprui33c/sprui33c.pdf.

[29] MathWorks. *C280x/C2802x/C2803x/C2805x/C2806x/C2833x/C2834x/F28M3x/F2807x/F2837xD/F2837xS/F2838x/F28004x ePWM*. [Online]. Accessed: Oct. 17, 2019. Available: https://www.mathworks.com/help/supportpkg/texasinstrumentsc2000/ref/c280xc2802xc2803xc2805xc2806xc2833xc2834xf28m3xf2807xf2837xdf2837xsf2838xf28004xepwm.html.

[30] MathWorks. *Modify Duty Cycle of ePWM Using DMA*. [Online]. Accessed: Oct. 17, 2019. Available: https://www.mathworks.com/help/supportpkg/texasinstrumentsc2000/ug/modify-epwm-using-dma.html

[31] Ferroxcube. *P36/22 Core Product Specifications*. [Online]. Accessed: Oct. 18, 2019. Available: https://www.ferroxcube.com/upload/media/product/file/Pr_ds/P36_22.pdf

[32] Ferroxcube. *3C91 Material Product Specifications*. [Online]. Accessed: Oct. 18, 2019. Available: https://www.ferroxcube.com/upload/media/product/file/MDS/3c91.pdf

[33] Ferroxcube. *Design Tool*. [Online]. Accessed: Oct. 28, 2019. Available: https://www.ferroxcube.com/en-global/design_tool/index

APPENDIX A

MAGNETICS TEST BED PCB

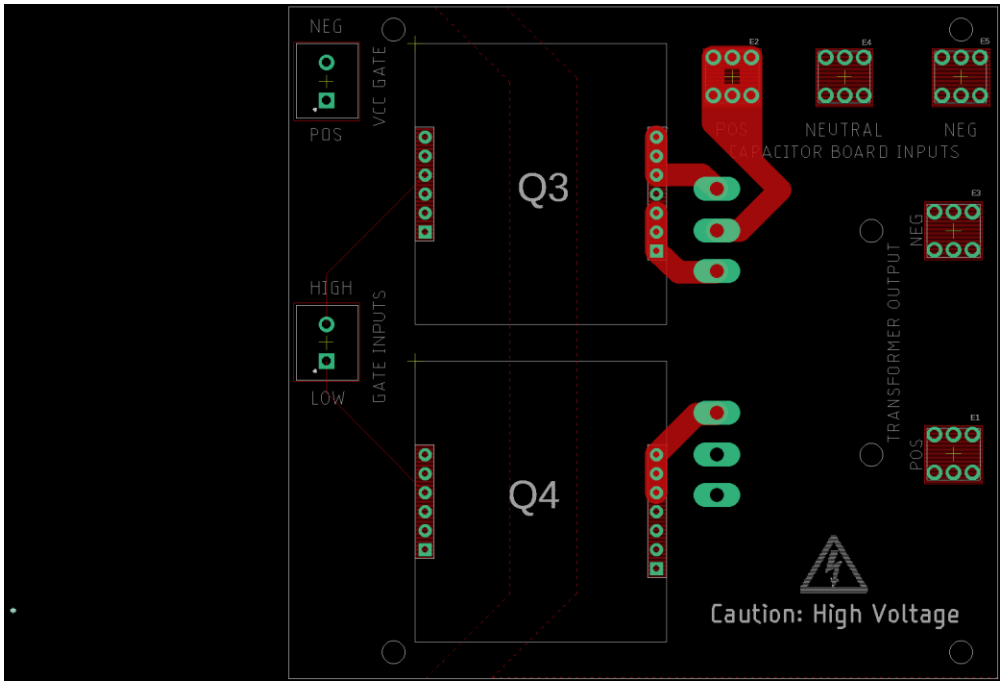

Figure A.1: Front of PCB

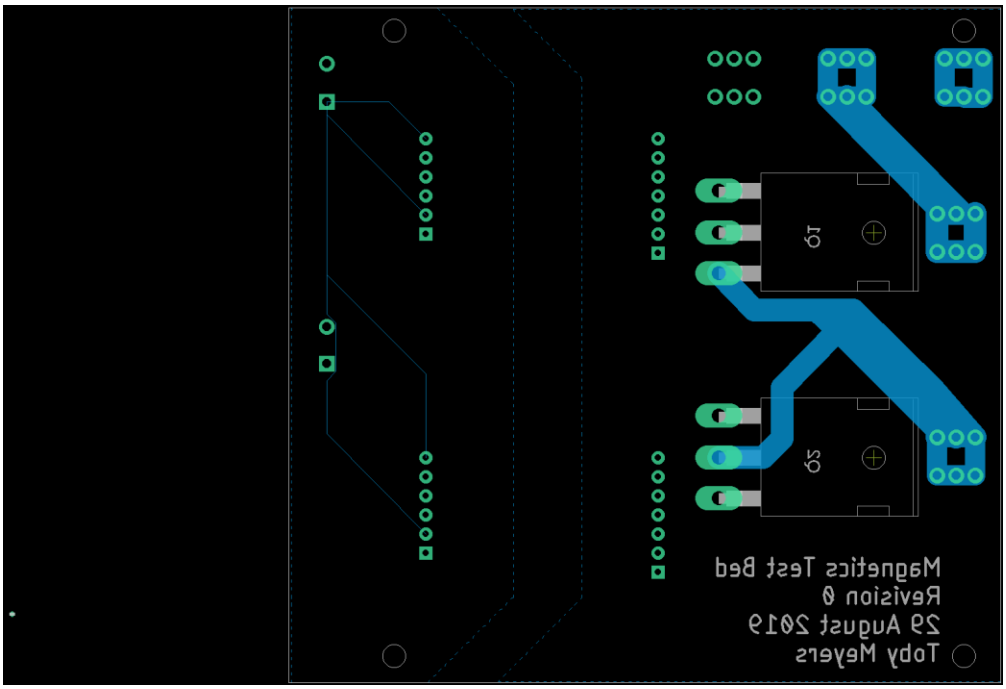

Figure A.2: Back of PCB

APPENDIX B

TRIPLE PULSE TEST CODE

```
//###########################################################
//
// FILE:   triplePulseTest.c
// TITLE:  Triple Pulse Test (for Magnetics Test Bed)
//
// AUTHOR:  Toby Meyers
// DATE:    23 September 2019
// UPDATED: 13 October 2019
//
// NOTE:    Make sure optimization settings are maxed out
//###########################################################

//
// Included Files
//
#include "F28x_Project.h"

//
// Defines
//
#define PWM1A      0
#define PWM1B      1

//
// Function Prototypes
//
void gpioSetup(void);
void pwmSignal(float, float);

//
// Main
//
void main(void)
{
   //
   // Define needed times
   // (Ton = Toff = Ts/2)
   // (Tmag = Ton + Tmag)
   // (Otherwise, negative DC Bias)
   //
   float Ts = 80.0f;
   float Tmag = 0.0f;

   //
   // init gpio outputs
   //
   gpioSetup();
```

```
   //
   // Call actual pwm function
   //
   pwmSignal(Ts, Tmag);

}//end main


void pwmSignal(float Ts, float Tmag)
{

   int i,j,magFlag;
   magFlag = 1;
   float Ton = Ts/2.0;

   // 2. Two pulses
   for (j = 1; j < 3; j++)
   {
      if (magFlag == 1 && Tmag > Ton)     // Magnetizing pulse
      {
         magFlag = 0;
         // 1. Magnetization pulse
         GpioDataRegs.GPACLEAR.bit.GPIO1 = 1;       // turn off bottom switch
         for (i = 0; i < 4; i++)                  // Deadtime (~240 ns)
            asm(" NOP");
         GpioDataRegs.GPASET.bit.GPIO0 = 1;         // turn on top switch
         DELAY_US(Tmag);                          // Stay on for Tmag

         //
         // Turn off half-bridge
         //
         GpioDataRegs.GPACLEAR.bit.GPIO0 = 1;        // turn off top switch
         for (i = 0; i < 4; i++)                  // Deadtime (~240 ns)
            asm(" NOP");
         GpioDataRegs.GPASET.bit.GPIO1 = 1;          // turn on bottom switch
         DELAY_US(Ton);                           // Stay off for Toff
      }
      if (magFlag == 1 && Tmag <= Ton)    //Standard pulse so all samples have 3 pulses
      {
         magFlag = 0;
         //
         // Turn on half-bridge
         //
         GpioDataRegs.GPACLEAR.bit.GPIO1 = 1;        // turn off bottom switch
         for (i = 0; i < 4; i++)                  // Deadtime (~240 ns)
            asm(" NOP");
         GpioDataRegs.GPASET.bit.GPIO0 = 1;         // turn on top switch
         DELAY_US(Ton);                           // Stay on for Ton
```

```
        //
        // Turn off half-bridge
        //
        GpioDataRegs.GPACLEAR.bit.GPIO0 = 1;        // turn off top switch
        for (i = 0; i < 4; i++)                     // Deadtime (~240 ns)
           asm(" NOP");
        GpioDataRegs.GPASET.bit.GPIO1 = 1;          // turn on bottom switch
        DELAY_US(Ton);                              // Stay off for Toff

      }

      //
      // Turn on half-bridge
      //
      GpioDataRegs.GPACLEAR.bit.GPIO1 = 1;          // turn off bottom switch
      for (i = 0; i < 4; i++)                     // Deadtime (~240 ns)
         asm(" NOP");
      GpioDataRegs.GPASET.bit.GPIO0 = 1;          // turn on top switch
      DELAY_US(Ton);                              // Stay on for Ton

      //
      // Turn off half-bridge
      //
      GpioDataRegs.GPACLEAR.bit.GPIO0 = 1;        // turn off top switch
      for (i = 0; i < 4; i++)                     // Deadtime (~240 ns)
         asm(" NOP");
      GpioDataRegs.GPASET.bit.GPIO1 = 1;          // turn on bottom switch
      DELAY_US(Ton);                              // Stay off for Toff

   }                        //end for

   // 3. Turn all off (open switches)
    GpioDataRegs.GPACLEAR.bit.GPIO0 = 1;          // turn off top switch
    GpioDataRegs.GPACLEAR.bit.GPIO1 = 1;          // turn on bottom switch
    DELAY_US(10);

}//end pwmSignal
```

```
void gpioSetup(void)
{

   //
   // Initialize device clock and peripherals
   //
   InitSysCtrl();

   //
   // Initialize GPIO and configure the GPIO pin as a push-pull output
   //
   InitGpio();
   GPIO_SetupPinMux(PWM1A, GPIO_MUX_CPU1, 0);
   GPIO_SetupPinOptions(PWM1A, GPIO_OUTPUT, GPIO_PULLUP);
   GPIO_SetupPinMux(PWM1B, GPIO_MUX_CPU1, 0);
   GPIO_SetupPinOptions(PWM1B, GPIO_OUTPUT, GPIO_PULLUP);

   //
   // Initialize PIE and clear PIE registers. Disables CPU interrupts.
   //
   DINT;
   InitPieCtrl();
   IER = 0x0000;
   IFR = 0x0000;

   //
   // Initialize the PIE vector table with pointers to the shell Interrupt
   // Service Routines (ISR).
   //
   InitPieVectTable();

   //
   // Enable Global Interrupt (INTM) and realtime interrupt (DBGM)
   //
   EINT;
   ERTM;

}//end gpioSetup
```